Limnol. Oceanogr., 58(6), 2013, 2185–2205

doi:10.4319/lo.2013.58.6.2185

Light and nutrient control of photosynthesis in natural phytoplankton populations from the Chukchi and Beaufort seas, Arctic Ocean

Molly A. Palmer,[1,*] Gert L. van Dijken,[1] B. Greg Mitchell,[2] Brian J. Seegers,[2,a] Kate E. Lowry,[1] Matthew M. Mills,[1] and Kevin R. Arrigo [1]

[1] Department of Environmental Earth System Science, Stanford University, Stanford, California
[2] Scripps Institution of Oceanography, University of California, San Diego, La Jolla, California

Abstract

During the 2010–2011 'Impacts of Climate Change on the EcoSystems and Chemistry of the Arctic Pacific Environment' project, we measured photosynthetic parameters in natural Arctic phytoplankton assemblages from the Chukchi and Beaufort seas. Water-column samples were taken from the near surface (3.1 ± 0.9 m) and subsurface (28 ± 10.3 m) at ~ 85 stations each year representing a wide range of ecological conditions, including under sea ice (UI) and in open water (OW). The physiological response of phytoplankton to light was used to assess photo-acclimation, photosynthetic efficiency, and maximum chlorophyll *a* (Chl *a*) normalized rates of carbon fixation. Phytoplankton from the subsurface were acclimated to lower irradiance, as evidenced by higher photosynthetic efficiencies (α^*), reduced mean absorption spectra ($\bar{a}^*$) associated with heavy pigment packaging, higher maximum quantum yields of photosynthesis (Φ_m), increased Chl *a* content (Chl *a*:POC), and higher potential growth rates (μ_m) than surface samples. In addition, phytoplankton growing in the UI subsurface had higher μ_m, increased Φ_m, and higher Chl *a* content, as well as reduced $\bar{a}^*$ compared with those found in OW. P^*_m did not vary between habitats despite vastly different nutrient and light conditions (averaging ~ 1 mg C mg^{-1} Chl *a* h^{-1}), except where nitrate exceeded > 10 mg m^{-3}, in which case P^*_m averaged 5–6 mg C mg^{-1} Chl *a* h^{-1}. Results from a stepwise regression analysis of photosynthetic parameters vs. environmental factors indicate that the concentration of inorganic nitrogen (significant relationships with P^*_m, α^*, Φ_m, μ_m, and Chl *a*:POC) and temperature at sample depth (a strong indicator of habitat type; significant relationship with β^*, $\bar{a}^*$, Φ_m, μ_m, and Chl *a*:POC) are the best predictors of photosynthetic variables. In addition, the amount of light available at sample depth significantly predicted both E_k and Chl *a*:POC. Our results suggest that it is the balance between light and nutrient availability in the various environments encountered in the seasonal sea ice zone that result in the pattern of photo-physiological data presented here. A significant proportion of primary production has now been observed to occur under the sea ice; therefore, our results may be a change from prior conditions in the region.

The Arctic Ocean exhibits extreme seasonality between the dark winter months and the 24 h sunlit summer, resulting in drastically varying light, temperature, and sea ice regimes throughout the year (Loeng et al. 2005). Marine primary production—the photosynthetic fixation of carbon dioxide (CO_2) by phytoplankton—in the Arctic is controlled by physical processes that modulate seasonal changes in light, nutrient, and temperature dynamics in the surface ocean (Sakshaug 2004; Carmack et al. 2006; Codispoti et al. 2009). To survive in areas of rapidly changing environmental conditions, phytoplankton must acclimate through physiological adjustments that balance photosynthesis with photo-protection, repair, and biosynthesis (Kirk 1994; MacIntyre et al. 2002; Falkowski and Raven 2007). Here, we investigate how these processes interact to control primary productivity in the Chukchi and Beaufort Seas.

In a typical seasonal cycle, Arctic phytoplankton begin to bloom in surface waters adjacent to the ice edge (marginal ice zone, MIZ) in late spring when sea ice starts to thin and retreat (Sakshaug 2004; Wang et al. 2005; Perrette et al. 2011). During this period, warming, runoff, and melt-water rapidly stratify the upper 20–50 m of the water column, creating a shallow stable mixed layer that is conducive for algal growth (Hill and Cota 2005; Loeng et al. 2005). This rapidly developing MIZ bloom quickly exhausts surface nutrients, particularly nitrate (NO_3), which is the primary limiting nutrient in the Arctic (Cota et al. 1996; Carmack et al. 2004; Codispoti et al. 2005). Following this, a subsurface chlorophyll *a* (Chl *a*) maximum (SCM) often forms at the nitracline, where NO_3 is still available and light is sufficient for growth, although it is unclear exactly how these SCM develop (e.g., whether they form in situ or are a relict feature of the previous MIZ bloom; Martin et al. 2010). In addition, phytoplankton may also bloom under sea ice (Legendre et al. 1981; Fortier et al. 2002; Mundy et al. 2009), an under-sampled habitat thought to be too inhospitable for growth, but where one of the most intense blooms ever recorded was observed in the Chukchi Sea in 2011 (Arrigo et al. 2012).

Several key processes precede bloom initiation and control bloom magnitude in the Arctic Ocean (Sakshaug 2004; Loeng et al. 2005): (1) Insolation slowly increases with solar elevation throughout the spring season into

* Corresponding author: mapalmer@stanford.edu

[a] Present address: University of Southern California, Los Angeles, California

summer, and a minimum light availability threshold must be surpassed before phytoplankton photosynthesis results in increased phytoplankton biomass (Sakshaug [2004] suggests a day length > 11–12 h for bloom initiation). (2) Thick sea ice and snow strongly attenuate and reflect incoming solar radiation, causing severe light limitation in the underlying water column that remains in effect until both snow and ice melt (Perovich 1998; Perovich and Polashenski 2012). (3) Nutrient availability is vital to bloom initiation; in the Chukchi Sea, local re-mineralization and winter mixing, plus the input of nutrient-rich Anadyr waters through the Bering Strait, pre-condition the region for high rates of phytoplankton productivity (Harrison and Cota 1991; Pickart 2004; Codispoti et al. 2005).

In recent decades, observed changes in the Arctic physical environment have profoundly affected marine primary productivity (Arrigo et al. 2008; Arrigo and Van Dijken 2011). Such changes include a > 30% reduction in the extent of the Arctic ice pack (Stroeve et al. 2005; Comiso et al. 2008), as well as sizeable reductions (> 40%) in average ice thickness (Rothrock et al. 1999; Lindsay and Zhang 2005) and the large-scale replacement of multi-year ice with thinner first-year ice (Nghiem et al. 2007; Maslanik et al. 2011). This has both lengthened the growing season and increased the area of open water suitable for phytoplankton growth (Arrigo et al. 2008; Pabi et al. 2008; Arrigo and Van Dijken 2011). Environmental changes have been particularly large in the Beaufort and Chukchi seas, especially in regard to sea ice thinning and retreat (Comiso et al. 2008; Shirasawa et al. 2009). In this region, the timing and intensity of the summer bloom are strongly affected by the dynamics of sea ice and water-column stabilization (Arrigo and Van Dijken 2004; Wang et al. 2005; Carmack et al. 2006).

In response to the changing physical environment (temperature, light), phytoplankton can vary molecular, morphological, and physiological traits that ultimately affect photosynthesis and growth rates (e.g., through photo-acclimation and photo-adaptation; *see* reviews in Falkowski 1992; Kirk 1994; Falkowski and Raven 2007). Phytoplankton balance light-harvesting needs with the ability to use the energy generated for growth (e.g., the quantum efficiency of photosynthesis), and thus energetically expensive tradeoffs within the cell are made (Kirk 1994; MacIntyre et al. 2002; Falkowski and Raven 2007). For example, in response to low irradiance, phytoplankton maximize photosynthetic rates by altering either the number of photosynthetic units (typically, by increasing photosynthetic pigment content) or the rate of electron turnover in the photosynthetic transport chain (Sukenik et al. 1987; Falkowski and LaRoche 1991; Falkowski and Raven 2007). However, nutrient limitation can affect the synthesis of pigment protein complexes (Falkowski 1992). For example, NO_3 limitation reduces growth rates and photosynthetic rates, both of which are linked to the reduction in protein synthesis through a reduction in functional reaction centers (Falkowski 1992). Temperature is thought to be a key factor limiting primary production in the Arctic, because photosynthetic rates are influenced by the activity of specific enzymes, whose activity is reduced at low temperatures (Li et al. 1984; Falkowski 1992; Morgan-Kiss et al. 2006).

In response to varying irradiance, the need to increase light-harvesting capability at low light is typically met with an increase in the synthesis of photosynthetic pigments, particularly Chl *a* (Falkowski and Owens 1980; Falkowski and LaRoche 1991). This increases photosynthetic efficiency (α^*) and the maximum quantum yield of photosynthesis (Φ_m), but decreases the maximum Chl *a*–normalized rate of photosynthesis, P^*_m (Kirk 1994; Falkowski and Raven 2007). It can also lead to a decrease in the mean Chl *a*–specific absorption coefficient ($\bar{a}^*$), because of the package effect, whereby adding pigment molecules reduces absorption efficiency per unit Chl *a* due to self-shading (Morel and Bricaud 1981). At higher irradiance, photosynthetic rates increase as cells synthesize more photosynthetic units to process the increased delivery of photons, and photosynthesis is controlled by the rate of electron transport (the concentration of photosynthetic pigment decreases as well; Falkowski and Raven 2007). However, exposure to supersaturating irradiances can damage photosynthetic reaction centers and lead to an increase in photo-protective pigments, both of which decrease the quantum efficiency of photosynthesis, α^*, and P^*_m (Falkowski and Raven 2007). Thus, within the limits of species-specific genetic potential (adaptation), photo-acclimation may result from changes in pigment concentrations and ensembles, and/or the structure of the photosynthetic apparatus (Falkowski 1980; Falkowski and Owens 1980; Falkowski and LaRoche 1991).

It is important to distinguish between genotypic changes that occur over longer timescales in response to low light, which is referred to as shade-adaptation, and phenotypic changes that occur over shorter timescales within a range constrained by genetic potential, which are called shade-acclimation (Falkowski and Raven 2007). This is because species-specific variations in photo-acclimation and adaptation can determine the presence or dominance of one phytoplankton group over others in polar marine waters, because phytoplankton groups can respond (acclimate) differently to variations in nutrient supply and irradiance on a timescale of hours to days and eventually years (Hill and Cota 2005; Kropuenske et al. 2009; Arrigo et al. 2010). The chronic exposure to low light in Arctic regions has given rise to the notion that most Arctic phytoplankton are shade-adapted and thus well-suited to exploit the extreme environmental conditions present in the MIZ (Platt et al. 1982; Subba Rao and Platt 1984; Kirst and Wiencke 1995). However, it is unknown whether there are differences in acclimation between phytoplankton groups from different environments. Moreover, it is unknown how future changes in sea ice and climate may affect the physical marine environment and thus phytoplankton distributions, although it has been suggested that a surface freshening would favor communities dominated by smaller algal species (Li et al. 2009). This has important implications for the entire food web as different taxa play different ecological and biogeochemical roles and link primary production to marine mammals, birds, fish, and benthic

communities (Stirling 1997; Grebmeier et al. 2006; Wassmann 2006).

We explored the physiological response of phytoplankton to different environmental conditions as part of the 2010–2011 'Impacts of Climate Change on the EcoSystems and Chemistry of the Arctic Pacific Environment' (ICESCAPE) project. We report here the results of short-term photosynthesis vs. irradiance (P-E) measurements, and focus our analysis on the photo-physiological differences between surface and subsurface populations, and between samples gathered in open water (OW; $<$ 25% ice) and under the sea ice (UI, $>$ 25% ice). Finally, we use transects extending in the direction of ice retreat from OW to $\sim$ 100 km into the ice pack as a proxy for the temporal evolution of an under-ice bloom, to explore changes in P-E parameters over time. Using the largest P-E data set published for this region, our goal is to characterize the patterns and processes controlling phytoplankton-based CO_2 uptake. It is critical, in this time of rapid ice melt and transformation, to provide a frame of reference for which to compare and predict future changes in biogeochemical carbon cycling for this region.

Methods

Study area—Hydrographic measurements and observations of the Chukchi and western Beaufort seas, Arctic Ocean, were performed onboard the United States Coast Guard (USCG) Cutter *Healy* from 18 June to 16 July 2010 and 28 June to 24 July 2011 (Fig. 1). Stations were primarily located over the continental shelf in waters $<$ 50 m deep (although several $>$ 1000 m deep stations were sampled in 2011), and were selected to represent the typical ecological and environmental conditions present in the region. In both years, we experienced spring-like conditions transitioning into summer, and encountered the southern margin of the sea ice zone between 67°N and 72°N (Fig. 1). In total, 253 P-E analyses were completed during ICESCAPE. These include 113 surface (3.1 $\pm$ 0.9 m depth) and 140 subsurface (28.0 $\pm$ 10.3 m depth) samples (Table 1), which were subsequently separated into two classes based on the concentration of sea ice (Table 2): 141 OW sites ($<$ 25% ice; 63 surface, 78 subsurface), and 112 UI sites ($\geq$ 25% ice; 50 surface, 62 subsurface; Table 2).

General sampling—Water-column casts were performed using a rosette with 12 30 liter Niskin bottles and equipped with a Sea-Bird Electronics SBE9*plus* Conductivity, Temperature, and Depth (CTD) sensor with a photosynthetically active radiation (PAR, 400–700 nm; QSP2300) sensor. Typically, CTD and PAR data were noisy in the first several meters of each cast and were removed. Water from Niskin bottles was poured immediately into triple-rinsed insulated plastic sample coolers and stored in the dark until analysis ($<$ 1 h). Analyses of Chl *a*, particulate organic carbon (POC), and nutrient concentrations were performed as described in Arrigo et al. (in press). Dissolved inorganic carbon (DIC) concentrations were measured as in Bates et al. (2005). At a few select stations (Table 3), more detailed light profiles were measured as in Frey et al. (2011; for the under-ice stations) and Arrigo et al. (in press; for the open-water stations).

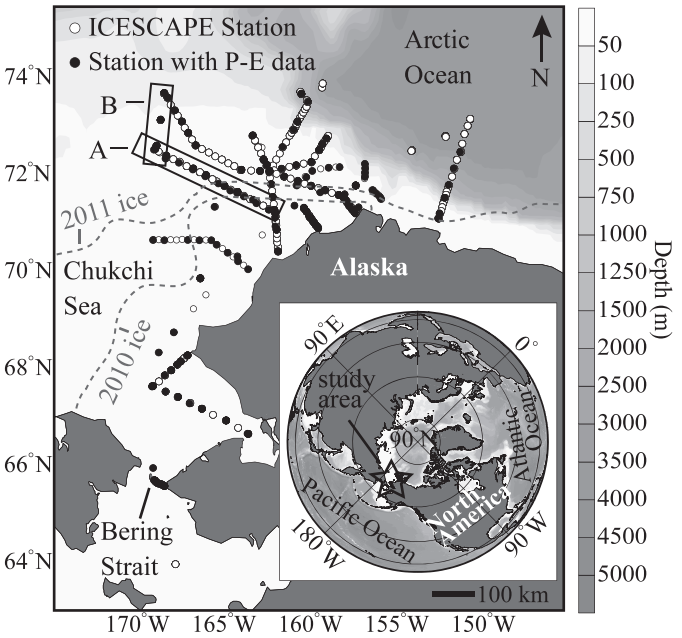

Fig. 1. Map showing the location of all 2010 and 2011 ICESCAPE stations (circles); filled-in circles indicate stations where P-E experiments were performed. Box A encompasses the main stations for the 2010 and 2011 Chukchi North transect (Sta. 71–89 for 2010, Fig. 3; Sta. 36–54 for 2011, Fig. 4); box B shows the extension into the sea ice for 2011 only (Sta. 55–57, Fig. 4). Dark grey is landmass; shading white to light grey is ocean bottom depth (scale at right). Dotted grey lines show ice edge at the beginning of sampling in 2010 (18 June) and 2011 (28 June).

%PAR, mixed-layer depth (MLD), and sea ice concentration—Because the upper few meters of PAR data from each vertical profile were unavailable after CTD post-processing, PAR just beneath the seawater surface (E_o) was determined by linearly extrapolating log-transformed PAR data from greater depths to the surface. PAR at each depth (E_z) was adjusted for variation in incident solar radiation (E_s) during the CTD deployment by normalizing E_z to E_s. The percent of surface PAR transmitted to each depth (%PAR) was calculated as $E_z : E_s$ divided by $E_o : E_s$ multiplied by 100. The euphotic depth (Z_{eu}) was defined as the depth where E_z was reduced to $\leq$ 0.1% of E_o. In Table 3, we also show the percent of incident downwelling PAR, E_s, transmitted to sample depth, E_z, calculated as $E_z : E_s$, using data from the UI and OW profiles (as opposed to the CTD; Frey et al. 2011).

Potential density (σ_θ) was calculated for each depth from temperature, salinity, and pressure using R code generated in the oceanographic toolbox. Upper mixed-layer depth (MLD, m) was calculated as the depth where σ_θ exceeded the surface value by 0.05 kg m^{-3}. In some cases, the water column was well-mixed and MLD could not be determined.

The concentration of sea ice at each station was estimated by a combination of (1) standardized visual observations made while at sea (over a 3 h period from the

Table 1. Environmental (A: physical and biological variables; B: chemical variables) and (C) photo-physiological data (mean ± SD) divided by depth class, surface (S) vs. subsurface (Sb). Shown in far right column are significant differences between depth classes (Kruskal–Wallis ANOVA). Temp. = temperature; PAR = photosynthetically active radiation; MLD = mixed-layer depth; Z_{eu} = euphotic depth; Chl *a* = Chlorophyll *a*; POC = particulate organic carbon; DIC = dissolved inorganic carbon; P^*_m = maximum Chl-*a* normalized rate of photosynthesis; α^* = photosynthetic efficiency; E_k = photo-acclimation parameter; β^* = photo-inhibition; $\bar{a}^*$ = mean absorption spectra; Φ_m = maximum quantum yield of photosynthesis; μ_m = maximum growth rate. Units for photo-physiological data: P^*_m: mg C mg Chl a^{-1} h^{-1}; α^* and β^*: mg C mg Chl a^{-1} h^{-1} (μmol quanta m^{-2} s^{-1})$^{-1}$; E_k: μmol quanta m^{-2} s^{-1}; $\bar{a}^*$: m^2 (mg Chl *a*)$^{-1}$; Φ_m: mol C (mol quanta absorbed)$^{-1}$; μ_m: d^{-1}; Chl *a* : POC : w : w.

	Surface (3.1 ± 0.9 m)		Subsurface (28.0 ± 10.3 m)		
	Mean ± SD	*n*	Mean ± SD	*n*	Stats: S vs. Sb (*p*)
A) Physical and biological variables					
Temp. (°C)	1.90±2.62	109	−0.38±1.71	140	<0.001
Salinity	30.71±1.98	109	32.11±0.71	140	<0.001
%PAR	57.7±20.4	104	2.9±7.2	135	<0.001
MLD (m)	11±6	108	11±6	136	—
Z_{eu} 0.1% (m)	34±17	80	37±18	96	—
Chl *a* (mg m^{-3})	5.02±10.35	113	7.28±8.78	140	<0.05
POC (μmol L^{-1})	27.6±36.1	103	31.1±29.2	133	—
B) Chemical variables					
NO_3+NO_2 (μmol kg^{-1})	0.30±1.03	109	4.21±4.60	139	<0.001
PO_4 (μmol kg^{-1})	0.59±0.17	109	1.09±0.40	139	<0.001
$Si(OH)_4$ (μmol kg^{-1})	5.94±6.09	109	14.01±13.04	139	<0.001
NH_4 (μmol kg^{-1})	0.13±0.26	109	0.52±0.73	139	<0.001
DIC (μmol kg^{-1})	1942.9±94.0	109	2079.8±76.9	140	<0.001
C) Photo-physiological data					
P^*_m	0.95±0.48	113	1.04±0.78	140	—
α^*	0.017±0.011	113	0.025±0.022	140	<0.001
E_k	69.6±45.9	113	50.1±36.1	140	<0.001
β^*	0.0005±0.0003	20	0.0007±0.0008	107	—
$\bar{a}^*$	0.0099±0.0047	105	0.0086±0.0051	134	<0.05
Φ_m	0.052±0.044	105	0.075±0.047	134	<0.001
μ_m	0.22±0.36	103	0.47±0.87	133	<0.001
Chl *a* : POC	0.008±0.010	103	0.019±0.032	133	<0.001

bridge), (2) analysis of photographs taken from the USCGC *Healy* camera mounted over the bridge at the time of CTD deployment, and (3) analysis of daily composites of satellite imagery from the Moderate Resolution Imaging Spectroradiometer-Aqua (National Aeronautics and Space Administration) and Special Sensor Microwave-Imager (National Snow and Ice Data Center) compiled during the cruise. Stations were placed into one of the predefined sea ice categories (OW or UI); the limit of 25% ice threshold was chosen because this best represented the two habitat types as encountered during the cruise and later defined by satellite imagery.

P-E measurements—P-E measurements were conducted using a short-term (1 h) ^{14}C-bicarbonate technique (Lewis and Smith 1983, as modified by Arrigo et al. 2010) at two depths per station (surface, 3.1 ± 0.9 m, and subsurface, 28 ± 10.3 m) using 20 light intensities ranging from 0 to 1500 (μmol quanta m^{-2} s^{-1}). P-E curves were fit using least-squares nonlinear regression to the model of Platt et al. (1980) as modified by Arrigo et al. (2010). For the P-E calculations, the measured seawater DIC concentrations were used prior to curve fitting. Briefly, the CO_2-fixation rate (P^*), at irradiance E was determined as

$$P^* = P^*_s\left(1 - e^{-\frac{\alpha^* E}{P^*_s}}\right)e^{-\frac{\beta^* E}{P^*_s}} - P^*_o \quad (1)$$

where P^*_s and P^*_o (mg C mg^{-1} Chl *a* h^{-1}) are the light-saturated maximum CO_2-fixation rates in the absence of photo-inhibition and at zero E, respectively; α^* is the photosynthetic efficiency, defined as the initial slope of the P-E curve (mg C mg^{-1} Chl *a* h^{-1} (μmol quanta m^{-2} s^{-1})$^{-1}$); and β^* is a measure of photo-inhibition (mg C mg^{-1} Chl *a* h^{-1} (μmol quanta m^{-2} s^{-1})$^{-1}$). Asterisks indicate Chl *a*–normalization. The maximum Chl *a*–specific CO_2- fixation rate, P^*_m, was then calculated as

$$P^*_m = P^*_s\left(\frac{\alpha^*}{\alpha^* + \beta^*}\right)\left(\frac{\beta^*}{\alpha^* + \beta^*}\right)^{\frac{\beta^*}{\alpha^*}} \quad (2)$$

P-E curve fits were accepted only if the coefficient of multiple determination, R^2yy(x), of the fit was > 60% (correlation of multiple correlation, Ryy(x), ≥ 75%), and/or the significance of the fit for each individual statistic had a p-value of ≤ 0.05. The photo-acclimation parameter, E_k, was then calculated from P-E data as P^*_m/α^*. The maximum biomass-specific growth rate (μ_m, d^{-1}) for a given sample was calculated as P^*_m divided by the POC : Chl *a* ratio for that sample.

Absorption coefficients and quantum yields—Spectral light absorption by particulates (phytoplankton and detritus) was determined onboard at 1 nm resolution (300–800 nm) using a dual-beam spectrophotometer (Perkin-Elmer-Lambda-19) equipped with an integrating sphere following standard ocean optics protocols as described in Mitchell et al. (2002). Absorption by phytoplankton (a_{ph}) was calculated as the difference between the particulate (a_p) and detrital (a_d) absorption coefficients (m^{-1}). The Chl *a*–specific spectral absorption coefficient for phytoplankton (a_{ph}^*, m^2 mg^{-1} Chl *a*) is a_{ph} normalized to fluorometrically determined Chl *a*. The spectrally averaged Chl *a*–specific absorption coefficient for phytoplankton ($\bar{a}^*$, m^2 mg^{-1} Chl *a*) was then calculated as

$$\overline{a}^* = \frac{\sum_{700}^{400} a_{ph}^*(\lambda) E(\lambda)}{\sum_{700}^{400} E(\lambda)} \quad (3)$$

where $E(\lambda)$ is the spectral output of the photo-synthetron light source.

The maximum quantum yield of photosynthesis, Φ_m, was calculated from α^* and $\bar{a}^*$ as

$$\Phi_m = \frac{\alpha^*}{43.2\overline{a}^*} \quad (4)$$

where 43.2 represents a unit conversion to mol C (mol quanta absorbed)$^{-1}$ (SooHoo et al. 1987).

Statistics—Data from 2010 and 2011 were pooled into a single data set after first using the Pearson Chi-square test to ascertain that P-E parameters determined for either ice category or depth sampled were not significantly different between years (all statistics were conducted using Statistica Software version 10, StatSoft).

To investigate how P-E parameters varied between the two depth classes (surface vs. subsurface) and the two ice classes (OW vs. UI), as well as between each ice class for a given depth (OW surface vs. UI surface, OW subsurface vs. UI subsurface), we used the nonparametric Kruskal–Wallis Analysis of Variance (ANOVA) test (α level: 0.05) because the data were not normally distributed (based on the Kolmogorov–Smirnov test, Shapiro–Wilks' W-test, and a visual inspection of the histograms for each variable; we also attempted the Box–Cox and log data transformations, but these did not correct the skew or make the data normal). The large sample size allows for a very robust statistical analysis regardless of the specific test performed, such that we are able to distinguish between small differences in the data. The conservative Bonferroni correction (α/n) was used for post-hoc multiple pair-wise comparison testing after the initial ANOVA was performed (using the Mann–Whitney test).

The association between explanatory environmental variables and P-E response variables was analyzed using multiple-regression analysis. We first used pair-wise comparisons of all environmental variables to eliminate redundancy in the data set. From this, we selected three key environmental factors for the regression: temperature, dissolved inorganic nitrogen (DIN, NO_3+NO_2), and the amount of PAR transmitted to sample depth (%PAR). Multiple forward-stepwise regression was then used to analyze the effect of these independent explanatory variables on P-E parameters using a significance cutoff of $p \leq 0.05$. The standardized multiple-regression coefficient (denoted b^* here) was used to compare the relative contribution of each independent variable in the prediction of the dependent P-E parameter. Finally, we used the nonparametric Spearman rank test to analyze the correlation between specific P-E parameters.

Results

Site description—Our cruise track progressed northward through the Bering Strait, along the Alaskan shelf, up through the Chukchi Sea, and eventually off the continental slope in the western Beaufort Sea (Fig. 1). Sea ice was encountered as far south as 68°N in 2010 and 71°N in 2011, including both pack ice and some land-fast ice along most of the Alaskan coast (Fig. 1 shows the location and shape of the ice edge at the beginning of sampling). In 2010, a large arm of pack ice from the central Arctic ice pack extended as far south as 68°N at the beginning of the cruise (18 June), but there were many large areas of open water open along the Alaskan coastline. This line of pack ice at 68°N formed the ice edge, which retreated in a northwesterly direction to 71°N by the end of the 2010 cruise (16 July), a distance of ~ 300 km in nearly 1 month.

In 2011, pack ice extended southward to 68°N a month prior (28 May) to sampling, forming the ice edge. This ice edge retreated in a northwesterly direction to 71°N (*see* 2011 ice line; Fig. 1) by the beginning of the cruise (28 June), and to 74°N by the end of the cruise (24 July), a distance of ~ 300 km. Thus, ice conditions (i.e., predominantly pack ice, with a consolidated ice edge) and rates of ice retreat (about 10 km d^{-1} in a northwesterly direction, or 300 km during the course of a 30 d sampling period; *see* Arrigo et al. [in press] for a more detailed description of ice retreat) during the course of the study were similar in both years, with the main differences being that we sampled 10 d later in 2011, and the ice edge was roughly 300 km further north at the beginning of sampling in 2011 than in 2010.

The majority of sea ice we observed in both years was first-year ice ~ 0.5–1.8 m thick, although we encountered several patches of very thick, ridged multi-year ice (2–4 m) near the Chukchi shelf-break (~ 74°N) in both years. Melt ponds were common in first-year ice, covering from 25% to 50% of the sea ice surface. The ice edge was generally very well-defined, although strong northerly winds occasionally advected ice southward, loosening the pack and reducing sea ice concentrations near the southern margin of the MIZ. In both years, a large under-ice phytoplankton bloom was observed in the region known as 'Chukchi North,' indicated by boxes A and B in Fig. 1 (the west side of box A was under sea ice, the east side was in open water; box B was completely under ice).

Differences between the surface and subsurface at all stations—Environmental conditions, Chl a, nutrients, and DIC: Environmental conditions at the surface (3.1 ±

Table 2. Environmental (A: physical and biological data; B: chemical data) and (C) photo-physiological data (mean ± SD) divided by ice class (OW and UI) and depth class (surface, S, and subsurface, Sb). Results from ANOVA between depths within each ice class are shown in the sixth column; the last column, Stats: OW vs. UI, shows results from ANOVA between ice classes for S and Sb samples (Kruskal–Wallis ANOVA; note: actual significance corrected as α/n, where $n = 4$, the number of post hoc texts performed, *see* text). Temp. = temperature; PAR = photosynthetically active radiation; MLD = mixed-layer depth; Z_{eu} = euphotic depth; Chl *a* = Chlorophyll *a*; POC = particulate organic carbon; DIC = dissolved inorganic carbon; P^*_m = maximum Chl *a*-normalized rate of photosynthesis; α^* = photosynthetic efficiency; E_k = photo-acclimation parameter; β^* = photo-inhibition; $\bar{a}^*$ = mean absorption spectra; Φ_m = maximum quantum yield of photosynthesis; μ_m = maximum growth rate. Units for photo-physiological data: P^*_m: mg C mg Chl a^{-1} h^{-1}; α^* and β^*: mg C mg Chl a^{-1} h^{-1} (μmol quanta m^{-2} s^{-1})$^{-1}$; E_k: μmol quanta m^{-2} s^{-1}; $\bar{a}^*$: m^2 (mg Chl *a*)$^{-1}$; Φ_m: mol C (mol quanta absorbed)$^{-1}$; μ_m: d^{-1}; Chl *a* : POC: w : w.

	Open water (OW)				
	Surface (S; 3.1 ± 0.9 m)		Subsurface (Sb; 28.0 ± 10.3 m)		
	Mean ± SD	*n*	Mean ± SD	*n*	OW stats: S vs. Sb (*p*)
A) Physical and biological data					
Temp. (°C)	3.41±2.18	63	0.28±1.94	78	<0.001
Salinity	31.35±1.12	63	32.17±0.71	78	<0.001
%PAR	60.1±22.3	61	3.7±9.6	73	<0.001
MLD (m)	12±7	58	12±7	74	—
Z_{eu} 0.1% (m)	32±14	40	35±18	50	—
Chl *a* (mg m^{-3})	2.75±5.40	63	7.74±10.48	78	<0.001
POC (μmol L^{-1})	20.5±21.3	58	33.7±35.3	75	<0.05
B) Chemical data					
NO_3+NO_2 (μmol kg^{-1})	0.40±1.25	63	3.58±4.18	78	<0.001
PO_4 (μmol kg^{-1})	0.56±0.18	63	1.00±0.38	78	<0.001
$Si(OH)_4$ (μmol kg^{-1})	5.29±5.51	63	10.14±9.76	78	<0.01
NH_4 (μmol kg^{-1})	0.17±0.32	63	0.58±0.85	78	<0.001
DIC (μmol kg^{-1})	1955.4±57.3	63	2070.0±80.1	78	<0.001
C) Photo-physiological data					
P^*_m	0.95±0.50	63	0.96±0.45	78	—
α^*	0.017±0.011	63	0.024±0.014	78	<0.001
E_k	67.4±37.0	63	47.3±24.3	78	<0.001
β^*	0.0006±0.0004	11	0.0006±0.0004	62	—
$\bar{a}^*$	0.0115±0.0050	60	0.0093±0.0047	73	<0.01
Φ_m	0.042±0.038	60	0.070±0.044	73	<0.001
μ_m	0.20±0.36	58	0.36±0.44	75	<0.001
Chl *a* : POC	0.007±0.008	58	0.015±0.012	75	<0.001

0.9 m depth; mean ± standard deviation) and subsurface (28.0 ± 10.3 m depth) differed significantly (Table 1A; Fig. 2). Temperatures were significantly greater in the surface than in the subsurface (Fig. 2A–D) and salinity was significantly lower (Table 1A). Mixed-layer depths were shallow, although most samples (> 95%) were collected from within the euphotic zone (Table 1A). Mean Z_{eu} for surface and subsurface samples differed slightly because valid data were not always available for both the surface and subsurface at every station. Surface samples were exposed to, on average, 20 times more downwelling irradiance than were subsurface samples (Table 1A).

Chl *a* concentrations were significantly more diminished in surface than in subsurface samples, although there was substantial variability at both depths because we sampled phytoplankton in many different phases of bloom development (Table 1A; Fig. 2I–L). Similarly, there was considerable variability in POC concentration such that surface and subsurface concentrations were not significantly different (Table 1A; Fig. 2M–P).

Inorganic nutrients were significantly less in surface than in subsurface waters. NO_3+NO_2 (Fig. 2E–H) and NH_4 concentrations were near zero in surface waters and much less than in the subsurface (Table 1B). PO_4 was also low in surface waters but not quite as depleted as NO_3+NO_2, and was nearly twice as high at depth (Table 1B). The most abundant nutrient was $Si(OH)_4$, which was more than twice as high in the subsurface than the surface (Table 1B). Similarly, DIC was significantly less in the surface than in the subsurface (Table 1B).

Photosynthetic parameters: There were significant differences between pooled surface and subsurface samples for almost all photosynthetic parameters studied (Table 1C; Fig. 3). Only two parameters were significantly higher in surface than subsurface populations: E_k was 39% greater in the surface than the subsurface, (Fig. 3I–L), and $\bar{a}^*$ was 11% higher (Fig. 3Q–T; Table 1C). In contrast, α^* was 47% more in subsurface than surface samples (Fig. 3E–H), and Φ_m was 46% greater (Table 1C). Similarly, subsurface maximum growth rates (μ_m) were more than double surface values (Fig. 2Q–T) and Chl *a* : POC ratios were 2.4 times greater (Table 1C).

There was no significant difference in P^*_m between surface and subsurface samples (Table 1C; Fig. 3A–D).

Table 2. Extended.

	Under ice (UI)					
	Surface (S; 3.1 ± 0.9 m)		Subsurface (Sb) (28.0 ± 10.3 m)			
	Mean ± SD	*n*	Mean ± SD	*n*	UI stats: S vs. Sb (*p*)	Stats: OW vs. UI (*p*)
A) Physical and biological data						
Temp. (°C)	−0.25±1.52	49	−1.20±0.83	62	<0.001	S, <0.001; Sb, <0.001
Salinity	29.94±2.48	49	32.04±0.72	62	<0.001	S, <0.001
%PAR	55.0±16.7	46	2.0±2.0	62	<0.001	—
MLD (m)	10±4	50	9±4	62	—	Sb, <0.05
Z_{eu} 0.1% (m)	36±20	40	39±18	46	—	—
Chl *a* (mg m^{-3})	7.88±13.89	50	6.69±6.05	62	<0.001	S, <0.001
POC (μmol L^{-1})	38.8±47.6	47	28.5±18.6	59	—	S, <0.001
B) Chemical data						
NO_3+NO_2 (μmol kg^{-1})	0.16±0.59	49	5.16±5.10	61	<0.001	Sb, <0.01
PO_4 (μmol kg^{-1})	0.65±0.15	49	1.20±0.41	61	<0.001	S, <0.01; Sb, <0.01
$Si(OH)_4$ (μmol kg^{-1})	7.33±7.15	49	18.95±14.99	61	<0.001	Sb, <0.001
NH_4 (μmol kg^{-1})	0.08±0.12	49	0.45±0.55	61	<0.01	—
DIC (μmol kg^{-1})	1925.8±127.2	46	2091.1±71.8	62	<0.001	S,<0.05; Sb, <0.05
C) Photo-physiological data						
P^*_m	0.95±0.47	50	1.15±1.05	62	—	—
α^*	0.018±0.011	50	0.027±0.030	62	—	—
E_k	72.3±55.5	50	53.6±46.9	62	<0.05	—
β^*	0.0005±0.0002	9	0.0008±0.0012	45	—	—
$\bar{a}^*$	0.0082±0.0042	45	0.0082±0.0059	61	—	S, <0.001; Sb, <0.05
Φ_m	0.066±0.048	45	0.081±0.050	61	—	S, <0.01
μ_m	0.25±0.36	44	0.48±0.38	59	<0.001	Sb, <0.01
Chl : POC	0.011±0.012	47	0.020±0.012	59	<0.001	S,<0.001; Sb, <0.05

Some of the highest P^*_m values observed were in the nutrient-rich Anadyr water in the Bering Strait (Fig. 3A–D), and in regions under the ice and near the ice edge where NO_3 concentrations (Fig. 2E–H) were high. Significant photo-inhibition, β^*, was observed in > 75% of the subsurface samples (Fig. 3O,P), whereas only 17.7% of surface samples exhibited signs of photo-inhibition (Fig. 3M,N; Table 1C).

Differences between surface and subsurface in open-water and under-ice areas—We explored variability within and between the open-water (OW) and under-ice (UI) samples in our study region using two separate ANOVA tests: for different depths within the same ice class and for similar depths between the two ice classes (Table 2).

Open water areas: Surface vs. subsurface: Environmental conditions, Chl a, nutrients, and DIC: OW areas displayed extensive variability between depths, with almost all environmental parameters exhibiting significant differences between the surface and subsurface (Table 2A–B). OW surface temperatures were the highest of all areas measured and were significantly higher than in the OW subsurface (Table 2A). Salinity was significantly reduced at the OW surface compared with the subsurface, and PAR was 16 times greater in the OW surface than subsurface (Table 2A). The MLD and Z_{eu} at stations from which OW surface and subsurface samples were collected did not significantly differ (Table 2A).

Although there was substantial spatial variability in OW samples, Chl *a* concentrations were > 3-fold lower in the OW surface than at the subsurface (Table 2A). Similarly, POC was significantly more diminished at the surface than in the subsurface in OW (Table 2A).

NO_3+NO_2 and NH_4 were both significantly less in OW surface than OW subsurface samples (Table 2B). PO_4 and $Si(OH)_4$ concentrations at the surface were approximately half the values in the subsurface (Table 2B). Similarly, DIC was reduced at the OW surface compared with the subsurface (Table 2B).

Photosynthetic parameters: Significant differences with depth were observed in most OW P-E parameters (Table 2C). One exception was P^*_m, which did not differ significantly between the OW surface and subsurface and averaged near ~ 1 mg C mg^{-1} Chl *a* h^{-1} for both depths

Table 3. Downwelling photosynthetically active radiation, PAR (E_z), at two depths (3 m and 28 m) in different ICESCAPE habitats and environments: under bare ice and under ponded ice (top) and in open water (bottom), with differing incident surface PAR (E_s), percent of incident above-surface PAR transmitted (Trans.) to depth (calculated as E_z/E_s), and bloom conditions (Chlorophyll *a*, Chl *a*; units mg m^{-3}). All irradiance units: μmol quanta m^{-2} s^{-1}. GMT = Greenwich Mean Time.

	Surface (3 m)						Subsurface (28 m)					
	Date (2011)	Time (h, GMT)	Chl *a*	E_s	E_z	Trans. (%)	Date (2011)	Time (h, GMT)	Chl *a*	E_s	E_z	Trans. (%)
Under ice (UI)												
UI—bare (Sta. 55)	04 Jul	22:22	17.4	644	56.3	8.71	04 Jul	22:24	3.12	643	0.127	0.020
UI—ponded (Sta. 55)	04 Jul	23:00	17.4	599	129	21.6	04 Jul	23:01	3.12	532	0.074	0.014
UI—bare (Sta. 56)	05 Jul	21:52	38.9	693	25.1	3.62	05 Jul	21:54	10.5	744	0.006	0.000
UI—ponded (Sta. 56)	05 Jul	22:34	38.9	683	99.6	14.6	05 Jul	22:36	10.5	707	0.005	0.002
UI—bare (Sta. 57)	06 Jul	22:11	0.91	847	89.2	10.5	06 Jul	22:13	6.72	854	1.39	0.163
UI—ponded (Sta. 57)	06 Jul	23:00	0.91	1142	445	38.9	06 Jul	23:01	6.72	1091	2.17	0.199
Open water (OW)												
OW (Sta. 25)	01 Jul	22:52	0.48	832	394	47.3	01 Jul	22:53	0.58	884	12.5	1.42
OW (Sta. 81)	09 Jul	21:25	5.01	1119	738	65.9	09 Jul	21:26	9.10	1101	5.95	0.405
OW (Sta. 113)	15 Jul	21:55	0.12	882	513	58.1	15 Jul	21:56	15.1	875	37.2	4.25

(Table 2C). Another exception was β^* (Table 2C), but it is important to note that this includes only 17.5% of OW surface samples vs. 79.5% of OW subsurface samples (e.g., these were the only samples where photo-inhibition was observed). α^* was 41% greater in the OW subsurface than at the surface (Table 2C). Similarly, Φ_m and μ_m were both $>$ 65% higher at the OW subsurface than in the surface (Table 2C). Chl *a*:POC was twice as high in the OW subsurface than in the OW surface (Table 2C). Conversely, E_k was 43% greater at the OW surface than in the subsurface (Table 2C). Similarly, $\bar{a}^*$ was 22% higher at the OW surface than in the subsurface (Table 2C).

Under ice areas: Surface vs. subsurface: Environmental conditions, Chl a, nutrients, and DIC: UI areas also differed significantly between depths for most environmental conditions sampled (Table 2A–B), although not as much as in OW. Temperatures under the sea ice were $< 0^\circ$C for both UI surface and subsurface samples, but UI subsurface areas were nearly a full degree colder than in the UI surface (Table 2A). Salinity was lesser in the UI surface than in the subsurface; the UI surface salinity was the lowest of all the habitats measured (Table 2A). The UI subsurface had a significantly lower %PAR than the UI surface (Table 2A). MLD and Z_{eu} did not differ significantly between UI surface and subsurface stations (Table 2A).

Chl *a* and POC varied substantially between depths in UI areas. Although displaying a wide range, Chl *a* was significantly higher in the UI surface than in the subsurface (Table 2A). POC also exhibited a very large range between the UI surface and subsurface, and no significant difference between depths could be ascertained (Table 2A).

Nutrients were significantly different between depths in the UI sites sampled, showing a general pattern of depletion in the surface and significantly higher concentrations at depth (Table 2B). NO_3+NO_2 and NH_4 exhibited the lowest concentrations, with surface values very near zero and subsurface values nearly five times higher (Table 2B). Similarly, PO_4 was very low in the UI surface, which was approximately half the UI subsurface concentration (Table 2B). Although $Si(OH)_4$ was much more plentiful than the other inorganic nutrients, concentrations were still more than twice as high in the subsurface than the surface (Table 2B). DIC in the UI surface was the lowest of all areas sampled, and was much lower than in the UI subsurface (Table 2B).

Photosynthetic parameters: In contrast to the OW areas, only the physiological variables E_k, μ_m, and Chl *a*:POC varied significantly between the UI surface and subsurface (Table 2C). E_k was significantly greater in the UI surface than the subsurface, while μ_m and Chl *a*:POC were both significantly reduced in the surface compared with the subsurface (Table 2C).

In contrast, there was no significant difference between the UI surface and subsurface for the variables P^*_m (both near 1 mg C mg^{-1} Chl *a* h^{-1}), α^*, β^*, $\bar{a}^*$, and Φ_m (Table 2C). However, a statistically significant β^* was observed only in 18% of UI surface samples, compared with 73% of UI subsurface samples.

Open-water and under-ice areas at the same depth—Environmental conditions, Chl a, nutrients, and DIC: Not surprisingly, conditions at OW sites differed in many respects from those at the UI sites ('S' for differences between OW and UI surface samples, or 'Sb' for differences between OW and UI subsurface samples, indicated in last column of Tables 2A–C). In OW, mean seawater temperature was $>$ 3°C warmer at the surface and $\sim$ 1.5°C warmer in the subsurface (Table 2A, last column) than in the UI. Salinity in the UI surface was the lowest of all habitats (Table 2A), and was significantly less than in the OW surface (Table 2A). Salinity did not differ significantly between the OW subsurface and the UI subsurface (Table 2A).

Because of greater light attenuation by sea ice, surface samples taken from UI sites received far less light than surface samples from OW sites (Table 3), regardless of Chl *a* concentration. Unfortunately, light profiles are not available for every station, and thus only data from a few example stations are presented in Table 3. In Tables 1 and

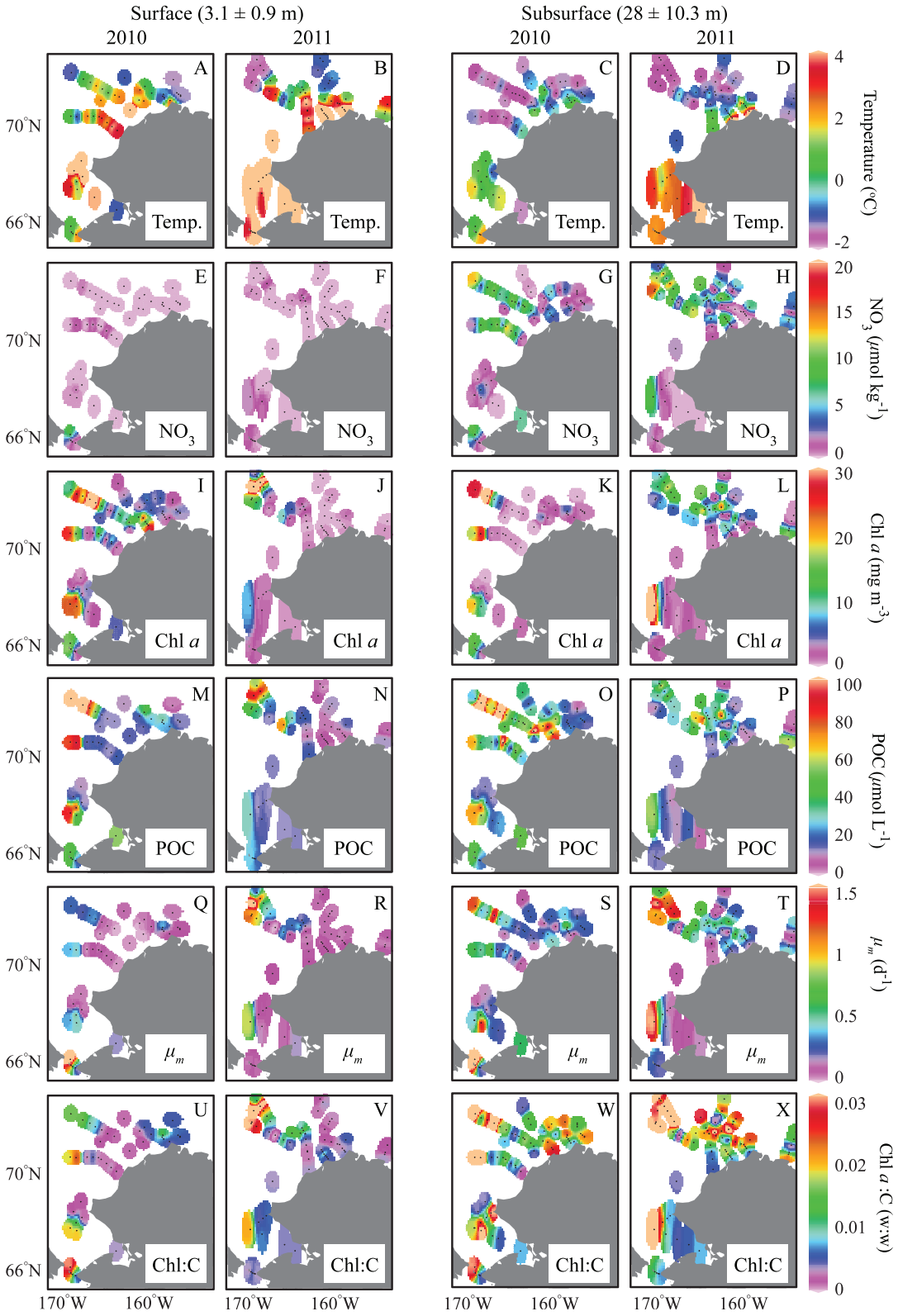

Fig. 2. Spatial plots of ICESCAPE environmental and associated variables in the surface (left two columns, sample depths average: 3.1 ± 0.9 m) and subsurface (right two columns, sample depths average: 28.0 ± 10.3 m), separated by year (2010 and 2011; note: color bars at right same for each row variable). Dark grey is Alaska landmass, white is Chukchi Sea and Arctic Ocean; *see* Fig. 1 for location info. Environmental variables (A–D) temperature; (E–H) nitrate; (I–L) chlorophyll *a*; and (M–P) particulate organic carbon. Also shown are: (Q–T) maximum growth rates; and (U–X) Chl *a* : POC ratios.

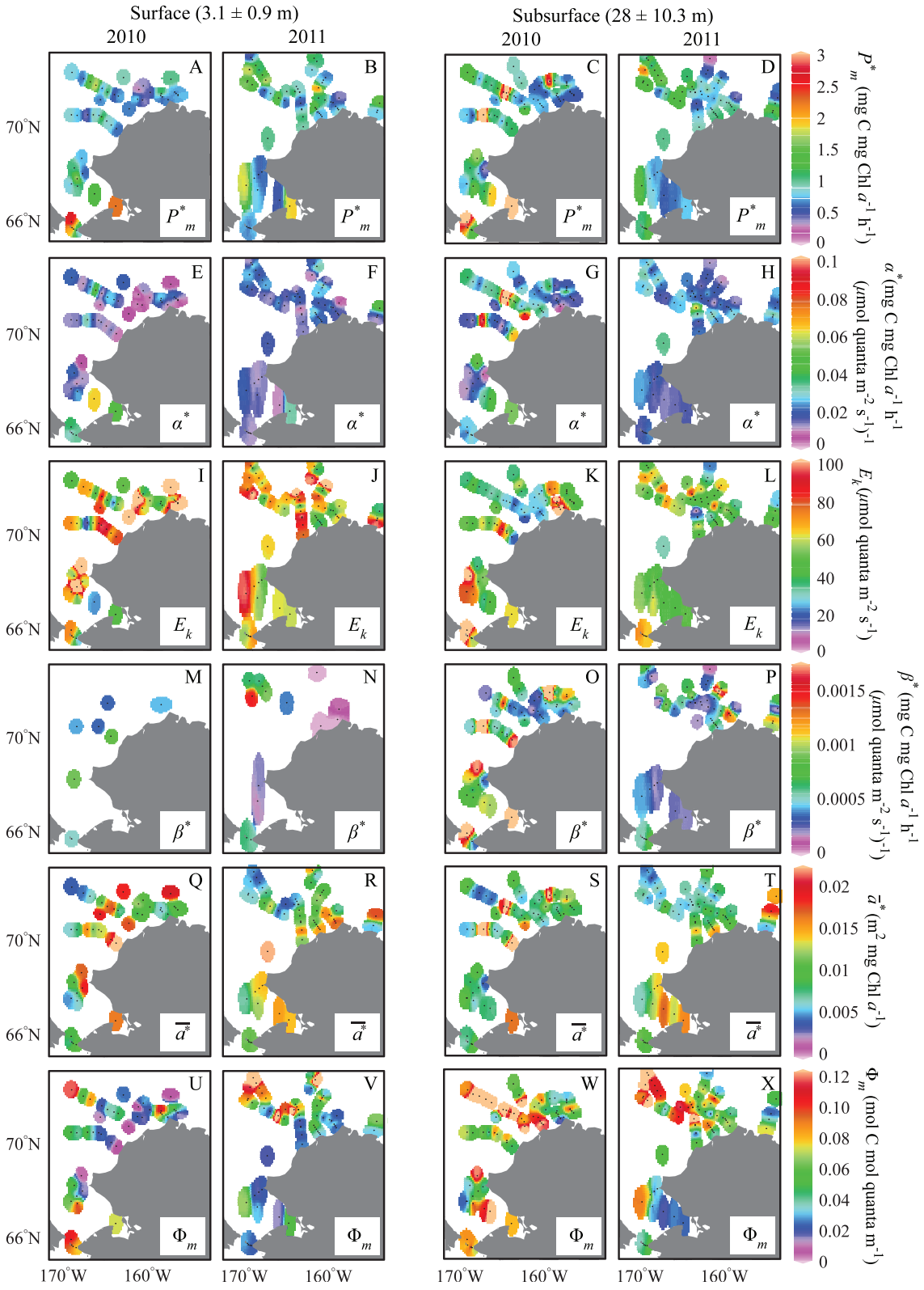

Fig. 3. Spatial plots of ICESCAPE photosynthetic variables in the surface (left two columns, sample depths average: 3.1 ± 0.9 m) and subsurface (right two columns, sample depths average: 28.0 ± 10.3 m), separated by year (2010 and 2011; note: color bars at right same for each row variable). Dark grey is Alaska landmass, white is Chukchi Sea and Arctic Ocean; *see* Fig. 1 for location info. Photosynthetic variables (A–D) P^*_m; (E–H) α^*; (I–L) E_k; (M–P) β^*; (Q–T) $\bar{a}^*$; and (U–X) Φ_m.

2, the light data are presented as %PAR calculated relative to the topmost values obtained by the PAR sensor on the CTD rosette, and thus no significant differences were observed between the %PAR reaching surface or subsurface zones in the two habitats (%PAR is calculated relative to the light just under the ocean surface in both habitats, and thus already includes attenuation by sea ice). Similarly, the calculated Z_{eu} did not differ significantly between OW and UI sites, while the UI exhibited a slightly (but significantly) shallower MLD than at the OW sites (Table 2A). Surface Chl *a* and POC both significantly increased at the UI sites, but did not differ between habitats in the subsurface waters (Table 2A).

NO_3+NO_2 and $Si(OH)_4$ were both significantly higher in the subsurface in UI habitats than in OW (Table 2B), but did not differ significantly between the two habitats in the surface. PO_4 was significantly higher in the UI than in OW both in the surface and the subsurface (Table 2B). NH_4 did not differ significantly between depths in the two habitats sampled, being very low everywhere (Table 2B). DIC was significantly greater in the OW surface than UI surface and was much less in the OW subsurface than UI subsurface (Table 2B).

Photosynthetic parameters: For P-E parameters and related variables, $\bar{a}^*$ and Chl *a*:POC were significantly different between the OW and UI sites at both the surface and subsurface (Table 2C, last column). Surface values of $\bar{a}^*$ were ~ 38% greater in the OW than the UI and subsurface values were ~ 13% more (Table 2C). Chl *a*:POC was significantly less in the OW than in the UI, by ~ 35% in the surface and 25% in the subsurface (Table 2C). In contrast, Φ_m only differed in the surface between the two habitats, and was 36% less in the OW than in the UI (Table 2C). Finally, μ_m only differed significantly between the two habitats in the subsurface, being ~ 33% greater in the UI than in OW (Table 2C). However, because UI sites receive far less light than the OW habitats (Table 3), the actual growth rate (μ) may seldom, if ever, be as high as μ_m calculated for many of the areas we sampled.

Temporal variability of P-E parameters: Chukchi North Transect—In both 2010 (Fig. 4) and 2011 (Fig. 5), we sampled a transect (Chukchi North) that extended from the open water off the coast of Alaska in a northwesterly direction for > 300 km into the sea ice zone in the direction of ice retreat, allowing us to observe how P-E parameters varied during different stages of a phytoplankton bloom (Fig. 1; boxes A and B, with the assumption that the bloom had developed under the sea ice and was thus progressively more advanced at further distances south of the ice edge; *see* below for more detail). In order to focus on the key patterns in P-E parameters revealed from this analysis, we combine both years together in the description of results below, because both years were similar in pattern with the exception that the bloom in 2010 was more developed than in 2011 (e.g., as evidenced by deeper and more severe nutrient depletion, greater and deeper concentrations of Chl *a* and POC, etc.). Although the years are lumped together below, we do highlight several key differences between years; please refer to Figs. 4, 5 for more detailed descriptions of P-E and environmental parameters along each transect. However, we also note that there could be differences between the years caused by inter-annual variability as well; a longer time series of data is needed to fully assess this possibility.

Open water: Physical and chemical environment: In both years, we encountered a strong SCM in the OW portion (0–100 km of Figs. 4, 5) of the transect (open water was on the east side of box A in Fig. 1). In this area, temperatures were relatively constant (~ 3–4°C) in the well-mixed upper layer, and declined sharply to −2°C below the pycnocline at ~ 28 m (Figs. 4A, 5A). A well-developed nitracline was present around 28 m as well, with virtually no NO_3 in the surface, increasing to 5–12 μmol kg^{-1} below the nitracline (Figs. 4B, 5B). Surface Chl *a* in the OW was near zero, but averaged 10–15 mg m^{-3} in 2010 and exceeded 30 mg m^{-3} in 2011 in the SCM at ~ 30 m depth (Figs. 4C, 5C). POC in OW was also higher in the SCM than in the OW surface, averaging 40–60 μmol L^{-1} (Figs. 4D, 5D). Based on the vertical patterns of Chl *a*, POC, oxygen (not shown), nutrients, and DIC along theses transects, the OW SCM in the southwest portion of both transects appeared to be in a relatively late stage of bloom development compared with the other areas sampled, most likely a remnant of an earlier bloom that had previously depleted surface nutrients and was migrating deeper with the nutricline (Figs. 4A–D, 5A–D).

Photosynthetic parameters: In the OW surface, P^*_m was ~ 0.5 mg C mg^{-1} Chl *a* h^{-1} in both years (Figs. 4E, 5E), and exhibited similar values (0.5–1.0 mg C mg^{-1} Chl *a* h^{-1}) in the OW SCM (Fig. 4E), except in one case in the 2011 transect where P^*_m was relatively high, near 1.5 mg C mg^{-1} Chl *a* h^{-1}, where the SCM was associated with the depth of the nitracline (Fig. 5E). Similarly, α^* and E_k in the OW SCM were comparable to OW surface values, although we note that values were slightly less in 2010 than 2011 (α^* range: 0.01–0.03 mg C mg^{-1} Chl *a* h^{-1} (μmol quanta m^{-2} s^{-1})$^{-1}$; E_k range: ~ 30 μmol quanta m^{-2} s^{-1} in 2010, 40–60 μmol quanta m^{-2} s^{-1} in 2011; Figs. 4F,G; 5F,G). Photo-inhibition (β^*) was apparent only in the OW SCM (Fig. 4H), and $\bar{a}^*$ was slightly higher at the OW surface than in the SCM in both years (Figs. 4I, 5I). Conversely, Φ_m was higher in the OW SCM than the OW surface in both years (Figs. 4J, 5J).

Ice edge: Physical and chemical environment: Continuing along the transect (in a northwesterly direction in box A; Fig. 1), in both years we first encountered sea ice in small pockets of mainly broken floes near the 100 km mark (ice concentration: top left box, Figs. 4, 5). Here (~ 100 km into transect) the pycnocline and associated nitracline had shoaled and surface temperatures were reduced (Figs. 4A,B; 5A,B at 100 km). The ice edge was encountered in both 2010 and 2011 at ~ 200 km from the start of the transect; sea ice concentration was ~ 100% and ice thickness was > 0.8 m. Close to the ice edge, the depth of the nitracline shoaled and surface temperatures were slightly warmer, abruptly transitioning to much colder waters under the sea ice (Figs. 4A,B; 5A,B). Similar to the OW sections of the transect, Chl *a* in the surface at the ice edge (~ 200 km) was very low (< 1 mg m^{-3}), but the SCM at the ice edge was shallower (near 15–20 m) than in the OW (Figs. 4C, 5C). Chl

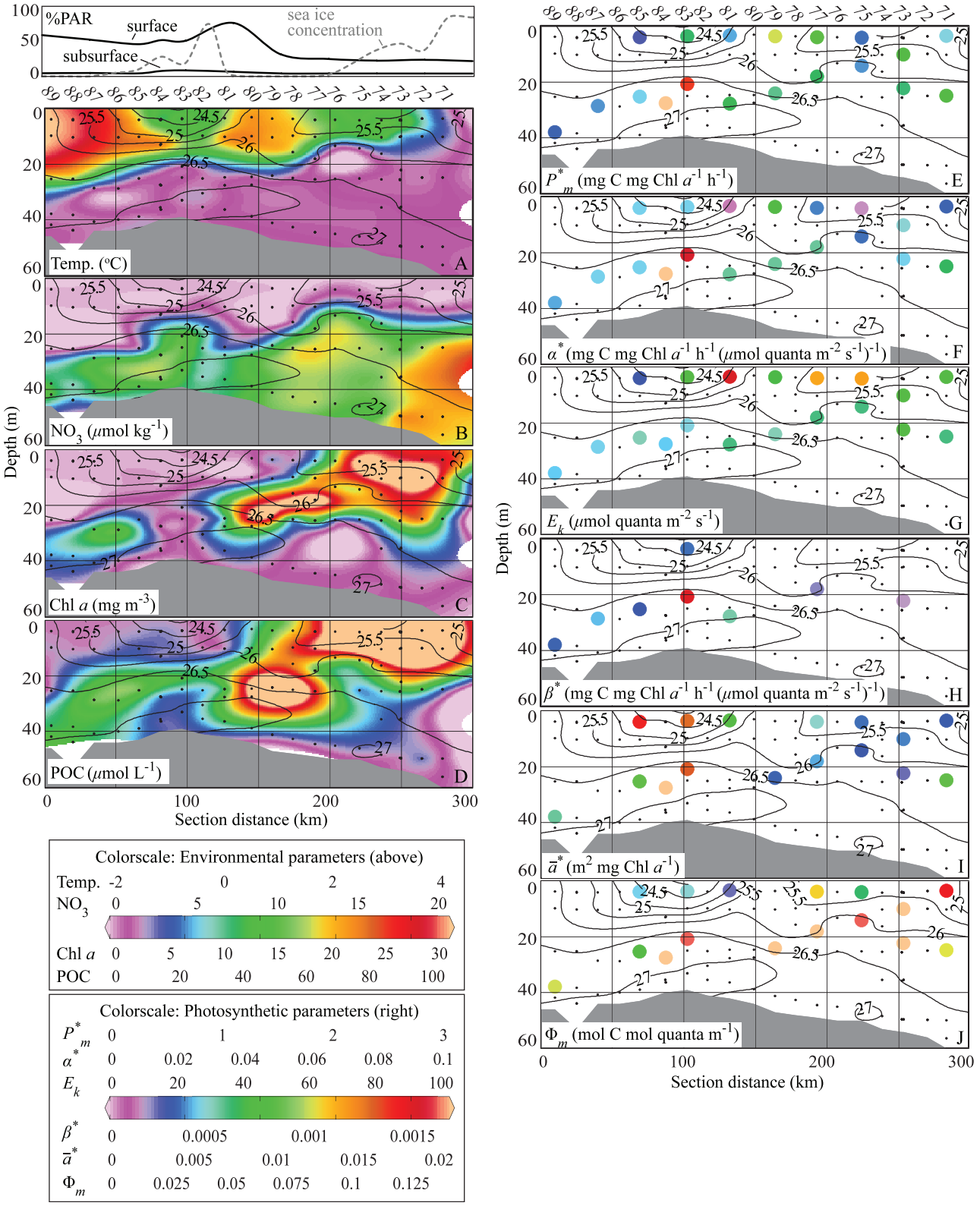

Fig. 4. (A–D) Environmental and (E–J) photosynthetic variables along the 2010 Chukchi North transect (Sta. 71–89; box A only in Fig. 1 with the section starting from the right most side of box A) vs. depth, sampled 06–07 July 2010. Dark grey is ocean bottom; light grey contours show potential density (units: kg m^{-3}); black dots show sample locations. Top left box shows sea ice concentration (grey line, 0–100%) and light penetration to sample depth (black lines, 0–100%) for surface and subsurface samples. Environmental variables and units: (A) temperature (Temp., °C); (B) nitrate (NO_3, μmol kg^{-1}); (C) chlorophyll *a* (Chl *a*, mg m^{-3}); and (D) particulate organic carbon (POC, μmol L^{-1}; color scales below). Photosynthetic variables and units: (E) P^*_m; (F) α^*; (G) E_k; (H) β^*; (I) $\bar{a}^*$; and (J) Φ_m (color scales bottom left).

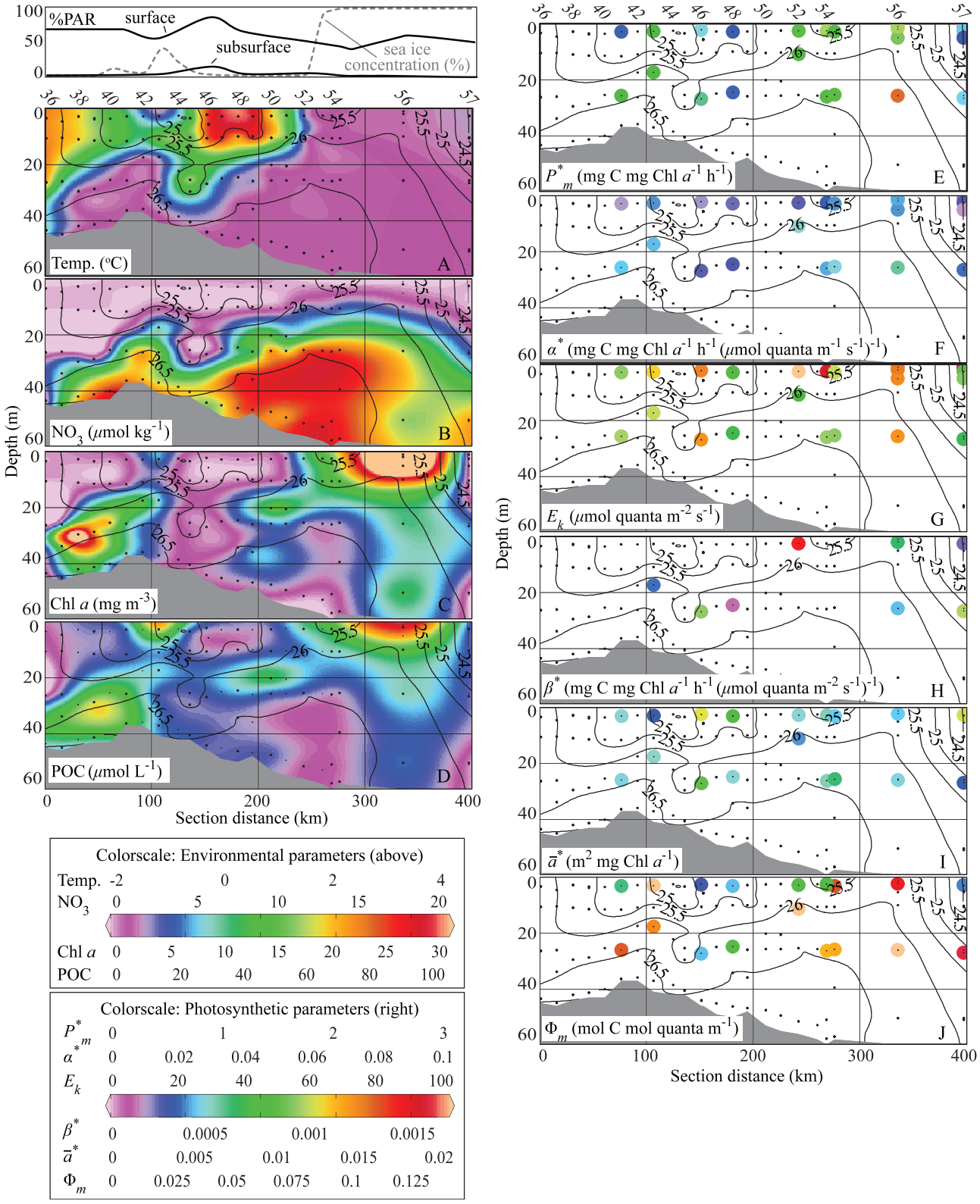

Fig. 5. (A–D) Environmental and (E–J) photosynthetic variables along the 2011 Chukchi North transect (stations 36–57; boxes A and B in Fig. 1) vs. depth, sampled 03–07 July 2011. Dark grey is ocean bottom; light grey contours show potential density (units: kg m^{-3}); black dots show sample locations. Top left box shows sea ice concentration (grey line, 0–100%) and light penetration to sample depth (black lines, 0–100%) for surface and subsurface samples. Environmental variables and units: (A) temperature (Temp., °C); (B) nitrate (NO_3, μmol kg^{-1}); (C) chlorophyll *a* (Chl *a*, mg m^{-3}); and (D) particulate organic carbon (POC, μmol L^{-1}; color scales below). Photosynthetic variables and units: (E) P^*_m; (F) α^*; (G) E_k; (H) β^*; (I) $\bar{a}^*$; and (J) Φ_m (color scales bottom left).

Table 4. Results from multiple stepwise regression analysis. Shown are standardized regression coefficients (beta), plus their individual significance (* = $p < 0.05$, ** = $p < 0.01$, *** = $p < 0.001$) as well as the details of the overall regression fit: significance (p), degrees of freedom (df), number of samples (n), correlation coefficient (r), and coefficient of multiple determination (r^2). Temp. = temperature; PAR = photosynthetically active radiation; P^*_m = maximum Chl-*a*-normalized rate of photosynthesis; α^* = photosynthetic efficiency; E_k = photo-acclimation parameter; β^* = photo-inhibition; $\bar{a}^*$ = mean absorption spectra; Φ_m = maximum quantum yield of photosynthesis; μ_m = maximum growth rate; Chl *a* = Chlorophyll *a*; POC = particulate organic carbon.

	Temp.	NO_3+NO_2	%PAR	p	df, n	r	r^2
P^*_m	—	0.19**	—	<0.01	1, 235	0.19	0.04
α^*	—	0.19**	−0.12	<0.001	2, 234	0.27	0.07
E_k	—	−0.08	0.20**	<0.001	2, 234	0.24	0.06
β^*	−0.20*	−0.17	—	=0.09	2, 116	0.20	0.04
$\bar{a}^*$	0.37***	—	—	<0.001	1, 225	0.37	0.13
Φ_m	−0.33***	0.19**	—	<0.001	2, 224	0.45	0.20
μ_m	−0.18**	0.43***	—	<0.001	2, 221	0.54	0.29
Chl *a* : POC	−0.23***	0.38***	−0.15*	<0.001	3, 220	0.61	0.38

a in the ice edge SCM exceeded 30 mg m^{-3} in 2010, and the high concentrations of Chl *a* extended over > 60 km along the transect (Fig. 4C). POC in the SCM at the ice edge in 2010 was similarly very high, averaging > 100 μmol L^{-1} (Fig. 4D). The pattern observed in 2011 was similar to that in 2010, except that the 2010 bloom had had more time to develop by the time we sampled, and thus Chl *a* and POC were slightly less in 2011 than in 2010 (Chl *a* in the 2011 SCM averaged only 10–15 mg m^{-3}, and POC averaged ~ 50 μmol L^{-1}; Fig. 5C,D). Based on our chemical and biological data, this transition zone between OW and UI likely represents an earlier bloom stage than that observed in open water, as nutrients were higher, less particulate material had accumulated, and Chl *a* was lower.

Photosynthetic parameters: At the ice edge, we saw more variability in P-E parameters than in the OW (Figs. 4E–J, 5E–J). P^*_m was slightly greater than in OW, near 1.5 mg C mg^{-1} Chl *a* h^{-1} (i.e., at 200 km along the transect in 2010 and 250 km in 2011; Fig. 5E), and both P^*_m and α^* showed a slight increase with depth (Figs. 4E,F; 5E,F). Similarly, $\bar{a}^*$ was low and Φ_m was higher at depth in both years (Figs. 4I,J; 5I,J). There was little to no photo-inhibition in either year near the ice edge, except for in 2011 where β^* in one surface sample was high (0.0015 mg C mg^{-1} Chl *a* h^{-1} (μmol quanta m^{-2} s^{-1})$^{-1}$) relative to the other samples (Figs. 4H, 5H).

One interesting difference between years in P-E parameters was observed near a patch of high NO_3 water (Fig. 4B) at the first ice floe at 100 km in 2010 (Sta. 83 and 84). At this site, P^*_m and α^* were both very high, the highest measured along both transects (> 3 mg C mg^{-1} Chl *a* h^{-1} and > 0.08 mg C mg^{-1} Chl *a* h^{-1} (μmol quanta m^{-2} s^{-1})$^{-1}$ for P^*_m and α^*, respectively; Fig. 4E,F), and E_k was low (~ 30 μmol quanta m^{-2} s^{-1}; Fig. 4G). Mean specific absorption spectra were also very high in this zone, as was Φ_m (Fig. 4I,J).

Under ice: Physical and chemical environment: Under > 50% ice cover, phytoplankton were in the earliest stages of bloom development, as shown by the highest observed concentrations of Chl *a*, POC, and NO_3 in the UI compared with the OW portions of the transects (Figs. 4A–D, 5A–D). In the most advanced bloom areas, NO_3 was severely depleted at the UI surface, but this did not extend vertically as deep as in the OW (i.e., the nitracline was shallowest here; Figs. 4B, 5B). In the UI, temperatures were cold (< 0°C) except for a few patches of recent ice break-up that showed some surface warming (Figs. 4A, 5A). UI Chl *a* was higher than in OW stations, reaching values > 30 mg m^{-3} for a large portion of the UI transect (Figs. 4C, 5C), with maximum concentrations near the ice–water interface. UI POC was similarly high, averaging 60–80 μmol L^{-1} and

Table 5. Correlation matrix using the nonparametric Spearman rank test for P-E parameters and associated variables. Bold indicates significance at the $p < 0.05$ level. P^*_m = maximum Chl-*a*-normalized rate of photosynthesis; α^* = photosynthetic efficiency; E_k = photo-acclimation parameter; β^* = photo-inhibition; $\bar{a}^*$ = mean absorption spectra; Φ_m = maximum quantum yield of photosynthesis; μ_m = maximum growth rate; Chl *a* = Chlorophyll *a*; POC = particulate organic carbon. Units for P-E parameters: P^*_m: mg C mg Chl a^{-1} h^{-1}; α^* and β^*: mg C mg Chl a^{-1} h^{-1} (μmol quanta m^{-2} s^{-1})$^{-1}$; E_k: μmol quanta m^{-2} s^{-1}; $\bar{a}^*$: m^2 (mg Chl *a*)$^{-1}$; Φ_m: mol C (mol quanta absorbed)$^{-1}$; μ_m: d^{-1}; Chl : POC: w : w.

	P^*_m	α^*	E_k	β^*	$\bar{a}^*$	Φ_m	μ_m	Chl *a* : POC
P^*_m	1.00	—	—	—	—	—	—	—
α^*	**0.55**	1.00	—	—	—	—	—	—
E_k	**0.23**	**−0.62**	1.00	—	—	—	—	—
β^*	**0.55**	**0.18**	**0.35**	1.00	—	—	—	—
$\bar{a}^*$	−0.09	−0.08	0.04	0.12	1.00	—	—	—
Φ_m	**0.48**	**0.79**	**−0.48**	0.07	**−0.64**	1.00	—	—
μ_m	**0.49**	**0.38**	−0.04	**0.19**	**−0.61**	**0.66**	1.00	—
Chl *a* : POC	**0.14**	**0.18**	−0.13	−0.09	**−0.69**	**0.54**	**0.91**	1.00

reaching values > 100 μmol L^{-1} over a large area (Figs. 4D, 5D). However, as described above for the case in OW, we note that the bloom sampled beneath the ice in 2010 was also at a slightly later stage of development than in 2011, as evidenced by the deeper Chl *a* penetration (> 30 m), greater and deeper accumulation of POC, and more severe NO_3 depletion in 2010 than in 2011 (Figs. 4A–D, 5A–D).

Photosynthetic parameters: In the under-ice bloom, P^*_m (Figs. 4E, 5E) averaged 1.0–1.5 mg C mg^{-1} Chl *a* h^{-1} (including the maximum value of > 2 mg C mg^{-1} Chl *a* h^{-1} measured where NO_3 was > 10 μmol kg^{-1}; Sta. 56, Fig. 5E). The initial slope of the P-E curve, α^*, was variable, but generally very low in the UI surface and slightly enhanced in the subsurface (near 0.02–0.04 mg C mg^{-1} Chl *a* h^{-1} (μmol quanta m^{-2} s^{-1})$^{-1}$; Figs. 4F, 5F). E_k was greater in the surface than subsurface, averaging ~ 70 μmol quanta m^{-2} s^{-1} compared with ~ 40 μmol quanta m^{-2} s^{-1} at depth; Figs. 4G, 5G). Values for mean specific absorption spectra ($\bar{a}^*$) were much less under the ice, suggesting intense pigment packaging associated with the very high Chl *a* in the bloom (Figs. 4I, 5I). Little to no photo-inhibition was observed in the under-ice samples (Figs. 4H, 5H). Finally, Φ_m showed a noticeable increase under the ice and at depth (Figs. 4J, 5J).

Regression analysis—To explore the environmental factors controlling variability in P-E parameters throughout our study region, we performed multiple stepwise regression analysis using the variables NO_3+NO_2, water temperature, and %PAR at the depth where samples were taken (Table 4), as well as correlation analyses between all P-E parameters (Table 5). Results indicate that the strongest predictor of P^*_m is the concentration of NO_3+NO_2. Similarly, NO_3+NO_2 was the best predictor of α^*; and although the overall regression fit was improved by adding %PAR into the equation, the coefficient itself was not significant (Table 4). Not surprisingly, %PAR was the best predictor of E_k (Table 4). Similar to α^*, the regression for E_k was improved by adding NO_3+NO_2 into the model, but the individual predictor was not significant even though the overall regression was (Table 4). Photo-inhibition, β^*, was most closely predicted by temperature, with a negative relationship between the two (Table 4). Adding the parameter NO_3+NO_2 also improved the overall fit of the regression for β^*, but we note that neither this nor the overall fit of the regression were significant (Table 4). The best predictor of $\bar{a}^*$ was temperature, with a strong positive relationship of (Table 4).

Φ_m was significantly correlated with two variables: temperature had a strong negative relationship with Φ_m, while NO_3+NO_2 had a positive relationship (Table 4). One of the strongest relationships revealed in the regression analysis was the strong positive association between μ_m and NO_3+NO_2 (Table 4). The regression also identified temperature as being a key negative predictor of μ_m. Interestingly, the only P-E parameter influenced by all three environmental variables was Chl *a*:POC (Table 4). Similar to μ_m, the strongest predictor of Chl *a*:POC was NO_3+NO_2. The other two regression variables both negatively influenced Chl *a*:POC, with temperature having a slightly stronger effect than %PAR.

Discussion

During ICESCAPE 2010–2011, we measured photosynthetic parameters over a range of environmental conditions, including under 0.5–1.8 m thick fully consolidated (~ 100% concentration) sea ice and in open water. Our values agree well with literature values for Arctic phytoplankton, particularly for 'shade-adapted' species growing at or near the ice edge, or in the OW at the SCM. In an early study of the Chukchi Sea, Hameedi (1978) measured assimilation numbers of ~ 1.5 mg C mg^{-1} Chl *a* h^{-1} in an actively blooming SCM (10–40 mg m^{-3} Chl *a*) near the ice edge in July–August. Similarly, Brugel (2009) reported a mean summertime P^*_m of 2.77 mg C mg^{-1} Chl *a* h^{-1} from the nearby Canadian Beaufort Sea, and Kirst and Wiencke (1995) give a range for the whole Arctic of 0.03–2.41 mg C mg^{-1} Chl *a* h^{-1}. Comparable to what we measured during ICESCAPE, Hill and Cota (2005) measured a summertime range for P^*_m of 0.60–1.10 mg C mg^{-1} Chl *a* h^{-1} for phytoplankton in the continental shelf and slope of the Chukchi and Beaufort seas in summer, and Palmer et al. (2011) report results from the same region of 0.93 mg C mg^{-1} Chl *a* h^{-1} and 0.71 mg C mg^{-1} Chl *a* h^{-1} from the UI and OW subsurface, respectively.

Interestingly, P^*_m in our study showed relatively little spatial variability and exhibited values near the lower end of the range typically attributed to Arctic phytoplankton (~ 1 mg C mg^{-1} Chl *a* h^{-1}). This includes surface and subsurface populations (Table 1C) both UI and in OW (Table 2C). In comparison, Harrison and Platt (1986) report an average P^*_m from 276 P-E experiments conducted in the eastern Canadian Arctic of 1.64 mg C mg^{-1} Chl *a* h^{-1} in samples taken from the 50% light level and 1.31 mg C mg^{-1} Chl *a* h^{-1} for samples from the 1% light depth (typically associated with the SCM), both of which are substantially higher than the mean values presented here.

Our results for α^* and E_k (Table 1C, 2C) fit well into the overall range for Arctic phytoplankton reported by Kirst and Wiencke (1995; E_k: 19–432 μmol quanta m^{-2} s^{-1}; α^*: 0.003–0.14 mg C mg^{-1} Chl *a* h^{-1} (μmol quanta m^{-2} s^{-1})$^{-1}$). Values for α^* and E_k from this study cannot be compared with those presented in Harrison and Platt (1986) because those authors measured light in W m^{-2} rather than μmol quanta m^{-2} s^{-1}, and conversion would require knowledge of the spectral quality of their light source. Hill and Cota (2005) do not present values for α^* and E_k. In comparison with studies specific to the Chukchi and Beaufort Sea region, our results for α^* and E_k agree well with those of Brugel (2009), who reported a mean summertime α^* of 0.054 (range: 0.003–0.113) mg C mg^{-1} Chl *a* h^{-1} (μmol quanta m^{-2} s^{-1})$^{-1}$ and an average E_k of 69 μmol quanta m^{-2} s^{-1}. Similarly, Palmer et al. (2011) report an average α^* of 0.019 mg C mg^{-1} Chl *a* h^{-1} and 0.014 mg C mg^{-1} Chl *a* h^{-1} (μmol quanta m^{-2} s^{-1})$^{-1}$ and E_k of 41 μmol quanta m^{-2} s^{-1} and 67 μmol quanta m^{-2} s^{-1} for SCM samples from OW and UI, respectively. In addition, the tendency in our data toward much more

frequent photo-inhibition in subsurface than in surface samples (Table 1C; Fig. 3M–P) was also observed by Harrison and Platt (1986) and Palmer et al. (2011).

Finally, our values of Chl *a* : POC (0.008–0.020 w : w; Table 1C and 2C) are similar to those of Platt et al. (1982), who measured Chl *a* : C ratios of 0.015 w : w and 0.026 w : w for samples from the 50% and 1% light levels, respectively. Similarly, our results for $\bar{a}^*$ and Φ_m from the SCM compare well with those reported in Palmer et al. (2011) from the nearby Canadian Beaufort Sea, which averaged 0.008 m^2 mg^{-1} Chl *a* and 0.044 mol C (mol quanta absorbed)$^{-1}$, respectively, in the UI habitat (data for OW SCM are estimates and not comparable).

Light and nutrient control of P-E parameters during ICESCAPE—In the Chukchi and Beaufort seas, light, nutrients, and temperature have been cited as important factors controlling photosynthetic rates of phytoplankton (Harrison and Platt 1986; Carmack et al. 2004; Tremblay et al. 2008). Particularly, the exposure to chronically low light levels (because of heavy cloud and ice cover, short summers, and low sun angles), and the high α^* and Φ_m and low P^*_m and E_k measured in most Arctic phytoplankton, are often cited as key evidence that Arctic phytoplankton are shade-adapted (or 'shade-acclimated,' depending on the timescale considered; Platt et al. 1982; Harrison and Platt 1986; Kirst and Wiencke 1995). For example, Platt et al. (1982) showed that in Baffin Bay, as in the Chukchi (Hameedi 1978; Lee et al. 2010) and Beaufort seas (Palmer et al. 2011), phytoplankton from the 1% light level had higher P^*_m and were more productive than phytoplankton from the 50% light level, indicating that shade-acclimated phytoplankton can perform well even at very low ambient light conditions if nutrients are in sufficient supply. Another example of this is in the North Water polynya, where complete consumption of NO_3 in the euphotic zone limited the photo-acclimation ability of phytoplankton (Tremblay et al. 2006). In addition, temperature may play a role in controlling P-E parameters, because at low temperatures ($< 0^\circ$C), the large investment in enzymes required to increase photosynthetic rates is too energetically expensive for most species (*see* Morgan-Kiss et al. 2006 for detailed review on temperature adaptation and acclimation in phytoplankton).

Although it is clear that light, nutrients, and temperature may all play a role in controlling the magnitude and range of P-E parameters in the dynamic ice-edge and open-water region of the summer phytoplankton bloom in the Chukchi Sea, it is of interest to determine which of these factors most influenced P-E parameters during ICESCAPE. The four main habitats we sampled during ICESCAPE (surface and subsurface communities both under the sea ice and in open water) differed with respect to temperature, light levels, and nutrient concentrations, and thus provide a model system in which to investigate the factors controlling phytoplankton photosynthesis and the range in P-E parameters.

Under the sea ice: Low values for P^*_m and E_k, and elevated β^* suggest that the low light conditions in the UI habitat imposed by the sea ice cover (Table 3) results in a shade-acclimated phytoplankton population, particularly in the subsurface. However, these populations also appear to respond to vertical variations in nutrients that develop over the course of the actively growing UI phytoplankton bloom. In the UI surface, severe nutrient depletion by the preceding UI bloom constrained P^*_m to relatively modest rates ($\sim$ 1 mg C mg^{-1} Chl *a* h^{-1}), despite higher light availability than in the UI subsurface at the SCM. In contrast, in the UI subsurface, light was greatly reduced but nutrients were in the greatest concentration of any of the four habitats sampled. Consequently, shade-acclimated phytoplankton in the UI subsurface were still able to maintain P^*_m rates of $\sim$ 1 mg C mg^{-1} Chl *a* h^{-1} despite these low light levels. The higher nutrient concentrations at the SCM likely allowed phytoplankton to synthesize more antenna pigments and photosynthetic units (increase Chl *a* : POC) for enhanced light absorption and produce more enzymes to facilitate faster rates of CO_2 fixation and growth (as evidenced by higher values for μ_m). The balance between low light and variable nutrient conditions under sea ice was used by Hill et al. (2005) to explain similar patterns of spring P-E parameters and total primary productivity and are consistent with the photo-acclimatory models presented in MacIntyre et al. (2002) and Falkowski (1980, 1992).

Supporting our conclusion that P-E parameters are controlled by both light and nutrients are the more rare cases where nutrients remained elevated within the euphotic zone. In these locations, we observed as much as 5-fold higher than average rates of P^*_m (*see* Sta. 56, Fig. 5E, for under 100% ice cover; or the marginal ice of Sta. 83–84 in Fig. 4E). In addition, the highest P^*_m values of both years (5–6 mg C mg^{-1} Chl *a* h^{-1}) were measured in nutrient-rich Anadyr water where NO_3 greatly exceeded 10 μmol kg^{-1} and phytoplankton were growing well within the euphotic zone. Thus, our data demonstrate that although phytoplankton maintain modest rates of photosynthesis due to low light availability under the sea ice, high nutrients can support higher maximal rates so long as sufficient light is available.

Our results suggest that the balance between higher light and lower nutrients at the surface and lower light and higher nutrients at the subsurface at the time of our cruises minimized the depth-related differences in P-E parameters. Essentially, the physiological benefits from having higher nutrient availability in the UI subsurface were counteracted by the very low light availability, such that the photo-acclimatory differences observed between surface and subsurface phytoplankton were little to no net change in P^*_m, and very little change in other P-E parameters. The primary difference we observed was an increase in light-harvesting pigments in low-light subsurface waters where nutrients were still available (Table 2C). The results from our regression analysis corroborate these findings, because NO_3+NO_2 exerted the strongest control on most P-E parameters (Table 4). It should also be noted that waters under the sea ice were not strongly stratified, allowing for the possibility that there was some exchange between the UI surface and subsurface, which may explain some of the similarity in many P-E parameters.

Open water: In contrast to the UI habitats, nearly all environmental and P-E variables differed significantly between the OW surface and subsurface (Table 2). This difference is likely related, at least in part, to differences in

stratification between the UI and OW environments. Because the OW region was more heavily stratified than UI, it is likely that there was little to no vertical exchange of phytoplankton or nutrients between the OW surface and subsurface. In addition, light availability in OW was much greater than in the UI habitats (Table 3), but surface nutrients were virtually exhausted in almost all OW surface sites sampled because of the earlier UI bloom, resulting in relatively strong vertical gradients. As such, our data indicate that in the OW, low surface nutrient availability results in P-E parameters that are controlled by the slow diffusion of NO_3 across the pycnocline. Nearly all the nutrients in OW are located at or below the SCM, so phytoplankton growth is similarly restricted to this depth; thus, subsurface OW phytoplankton must also be shade-acclimated, because light is much lower at the SCM than at the surface (Tables 2A, 3). Shade acclimation in the SCM was evidenced by higher values for α^*, Chl a : POC, and β^* and a lower E_k and $\bar{a}^*$ (due to pigment packaging) than in surface samples (Table 2C).

However, the light levels at the SCM were higher in the OW than the UI habitat (Table 3), so that phytoplankton at the SCM in OW had to devote fewer resources to acquiring light than in the UI habitat. This is seen particularly clearly by the lower Chl a : POC in OW at both the surface and subsurface. Hence, OW phytoplankton likely synthesized fewer photosynthetic pigments and were less shade-acclimated than those growing in the UI.

As in the UI habitat, the pattern in P-E parameters in OW was also clearly related to nutrient concentrations, which were higher at the SCM than at the surface. As a result, Φ_m and μ_m were both higher in the OW subsurface, despite the lower light availability (Table 2C). In addition, nutrient availability was generally lower in OW habitats than UI habitats and μ_m was lower as well (Table 2C). Thus, the OW data suggest that the counteracting effects of lower nutrients but higher light availability in OW habitat results in a range of values for P-E parameters (especially P^*_m) similar to that measured in the UI environment.

Temperature: Finally, we note that the influence of temperature on P-E parameters seemed to be small, because the highest rates were associated with the coldest temperatures (Table 2C). This is contrary to what would be expected if temperatures controlled primary productivity through the regulation of enzymatic activity (Li et al. 1984). Although the regression analysis does show that temperature was a key factor in the prediction of five of the eight parameters analyzed, we suggest that the importance of the temperature term was exaggerated because of its tendency toward co-variation with both light (positively correlated) and nutrient concentration (inversely correlated). Because variations in temperature in our study region were generally small, the magnitude of thermodynamic and/or kinetic control of physiological rate processes was likely small as well. Nonetheless, further research into the synergistic effects of low-light and low-nutrient conditions on phytoplankton that thrive in permanently cold environments is needed to fully understand the role that temperature plays in influencing photosynthetic response (Morgan-Kiss et al. 2006).

Ecological implications of variability in P-E parameters—An important implication of our results is that the observed spatial patterns in P-E parameters may be a unique feature of the thinning ice cover now present in the region. In the past, either massive phytoplankton blooms under the ice occurred and were not observed, or they did not occur. If the latter, then the mere fact that phytoplankton can now bloom under the ice is more likely due to different environmental conditions rather than different photosynthetic characteristics. If the former, we would expect that, with the thicker, more consolidated ice with and higher snow-covered ice that historically covered the region, phytoplankton blooming under the ice would have photosynthetic characteristics similar to those presented in Cota (1985), which measured phytoplankton from the bottommost layer of sea ice (1.8 m thick, snow 2–30 cm) in late May (these are the only under-ice P-E parameters from this region of the Arctic that we have been able to find). P^*_m values in their samples were $>$ 20 times lower than those presented here (average: 0.050 mg C mg^{-1} Chl a h^{-1}), even with no snow cover (Cota 1985; note: these data are for ice algae, and the comparison should be made with caution). Thus, it seems reasonable to assume that the photosynthetic parameters measured during ICESCAPE from under-ice phytoplankton in a massive bloom situation are a unique feature of the conditions now present in the region, and the biggest change has been in the sea ice field. With thinner, first-year ice largely dominating the ice types covering the ICESCAPE study region, plus the vast proliferation of melt ponds, light penetration to the surface waters under the ice cover has increased 4-fold (Perovich and Polashenski 2012), and phytoplankton now bloom under the sea ice (Arrigo et al., in press) with greater efficiency and at higher rates than ever before. Light under the ice is lower than in the near-surface waters of the ice edge and in ice-free waters (Table 3), and thus shade-adapted phytoplankton growing under sea ice must be able to increase their ability to harvest light in order to achieve the large levels of biomass we observed. Ultimately, this cannot be done without sufficient nutrients, which explains why P-E parameters are so tightly coupled to NO_3 availability, and why P^*_m is limited to such a narrow range.

Additionally, because phytoplankton that grow within the UI bloom are physiologically adapted to low-light conditions, they are likely well-suited to exploit the similar low-light and high-nutrient conditions in the OW SCM once the sea ice retreats. In fact, our data suggest that because under-ice phytoplankton are already acclimated to grow at low-light conditions, these phytoplankton may grow faster and perform better photosynthetically at the OW SCM than surface phytoplankton originating in a well-lit MIZ. Furthermore, the ability of shade-acclimated phytoplankton to grow beneath the sea ice and consume most of the surface nutrients while the region is still ice-covered means that phytoplankton growth in the normally productive surface waters of the MIZ may be reduced compared with what it would have been if nutrients were more abundant in the period of time immediately following ice retreat (although it is unclear how the physical environment of the MIZ would also affect nutrient

availability). Eventually, regions of the Arctic with diminishing ice cover, such as the Chukchi Sea, may shift away from a primarily MIZ-type bloom cycle (Perrette et al. 2011) to one that is dominated by under-ice phytoplankton blooms.

The observed shade-acclimation of phytoplankton in our study region and high potential growth rates under the ice illustrates how nutrient availability can regulate the ability of phytoplankton to cope with low-light conditions. This is consistent with previous studies of the region (Carmack et al. 2006; Tremblay et al. 2008; Lee et al. 2010), which suggested that P-E parameters in the ice-associated region of the Chukchi Sea vary primarily based on nutrients, because shade-adapted phytoplankton can utilize light at much lower levels than can their high-light adapted counterparts. However, our results do not as closely support the temperature- and light-control theory of some earlier studies of the region (Li et al. 1984; Harrison and Platt 1986; Harrison and Cota 1991), hinting at the possibility that recent changes in sea ice and environmental conditions may be altering phytoplankton growth and photosynthesis in several fundamental and important ways, and/or that the data sets are not as comparable as we are assuming in this study (e.g., possibly because of biases in sampling location, timing, methodology, etc.). More work is needed to fully understand the effects of changing environmental conditions on P-E parameters of natural phytoplankton populations from this dynamic region.

Finally, it is also interesting to consider whether our sporadic observations of high P^*_m associated with high NO_3 and sufficient light have important consequences for the annual bloom cycle. Early in the Arctic spring, light will always be low, and thus P^*_m will always be controlled by light availability (especially under-ice cover) regardless of temperature or nutrient concentrations. However, incident irradiance increases rapidly in spring, and light transmission through the sea ice becomes sufficient to support net phytoplankton growth when surface NO_3 concentrations are still high. Indeed, model results indicate that most of the Chukchi shelf contains > 10 μmol kg^{-1} NO_3 (Zhang et al. 2010) under the ice prior to the spring bloom due to wintertime mixing, transport, and re-mineralization (the main exception being the waters associated with the Alaska Coastal Current). Thus, it is likely that phytoplankton communities over much of the Chukchi Sea had substantially higher P^*_m prior to our ICESCAPE cruises than we present here. By under-sampling the sea ice zone in spring, we are missing a key component of the seasonal cycle of primary productivity and may be underestimating annual production (Pabi et al. 2008; Arrigo and Van Dijken 2011; Perrette et al. 2011). Although rapid nutrient drawdown under the ice means that these potentially high rates of early season P^*_m are likely to be short-lived, the very high values for P^*_m observed in ICESCAPE during this period suggests we may need to more seriously consider under-ice primary production as the Arctic sea ice cover continues to recede and thin.

A new paradigm of primary productivity in the Chukchi Sea—Based on the multitude of data collected during the ICESCAPE program, we see a new pattern emerging in the seasonal cycle of phytoplankton growth in the Chukchi Sea. This is described in detail in Arrigo et al. (in press). Below, we describe how P-E parameters fit into this new bloom paradigm. The different phases can be summarized as follows:

(1) Early in the season, wintertime nutrient replenishment and regeneration increases nutrient concentrations throughout the water column, with low light preventing net photosynthesis. As solar elevation increases throughout the spring, the presence of extensive sea ice results in little to no light penetration to the surface ocean, and phytoplankton do not grow (Legendre et al. 1981; Fortier et al. 2002).

(2) Once the snow has melted and light beneath the 100% sea ice cover exceeds the compensation irradiance for phytoplankton net growth, the spring bloom develops *under the sea ice* (*see* Arrigo et al., in press for more detailed description and biogeochemical evidence of bloom evolution). Melt pond formation enhances light penetration through the ice, accelerating the time to reach the light threshold necessary for photosynthesis (Frey et al. 2011). This is aided by shade-adaptation by phytoplankton: our data show that low light availability initially limits P^*_m, but nutrients are high so phytoplankton can synthesize additional Chl *a*, allowing them to absorb more of the available light (Tables 2A, 2C; Figs. 4C, 5C). This large investment in light-harvesting machinery increases the photosynthetic efficiency, growth rate, and accumulation of phytoplankton biomass under the ice (Tables 2A, 2C; Figs. 4, 5). Nutrients begin to be depleted from the surface waters under the ice pack (Table 2B; Figs. 4B, 5B).

(3) As the season progresses, UI phytoplankton utilize the enhanced light (both from increased solar intensity in the summer as well as thinner sea ice) to extend deeper in the water column, depleting nutrients at increasingly greater depths (Figs. 4C, 5C). Our data show that phytoplankton may grow to depths of up to 30 m under the ice as they move deeper to exploit nutrients, and also that an SCM may also begin to develop once nutrients are exhausted in the surface layers (Figs. 4C, 5C). The highest rates of P^*_m are associated with depths where NO_3 is still available and light is sufficient for photosynthesis (Figs. 4E, 5E). The phytoplankton blooming under the ice are photo-acclimated to the low-light conditions and maintain comparable levels of P^*_m, α^*, $\bar{a}^*$, and Φ_m between the surface and the SCM (Table 2C; Figs. 4E–J, 5E–J). Importantly, the phytoplankton community growing near the surface has high light availability, whereas the community growing in the subsurface has high nutrient availability; it is this distinction that creates the key differences in many of the P-E parameters (Table 2).

(4) Finally, the ice melts and retreats, stratifying the water column and isolating the nutrient-poor surface waters from nutrient rich waters below (*see* density contours in OW portions of Figs. 4 and 5; Arrigo et al. in press). As described in Arrigo et al. (in press), it may be that in areas where there was significant phytoplankton production under the ice, no bloom develops in surface waters of the MIZ because of depleted nutrients, and the SCM in the MIZ and OW zone could be considered a remnant under-ice bloom. Our photo-physiological data are consistent with this idea, because it shows that phytoplankton that had been growing in the low-light UI environment are already acclimated to the low-light conditions of the OW SCM: the OW subsurface communities have higher growth rates, Chl *a*:POC ratios, Φ_m, and α^*, and lower $\bar{a}^*$ than those in the OW surface (Table 2C; Figs. 4F, I–J; 5F, I–J). The final phase of this new paradigm described in Arrigo et al. (in press) is that as the OW SCM becomes progressively deeper throughout the season, shade-acclimated phytoplankton continue to grow well at depths where both light and nutrients are available (Figs. 4C, 5C).

Future research—Phytoplankton from the UI and OW SCM in the Chukchi and Beaufort seas were more shade-adapted, more efficient per light absorbed at producing a photochemical reaction, and were growing at a faster rate than phytoplankton in surface waters (Fig. 3; Tables 1–2). Our data suggest that these adjustments are related to the significant increase in light-harvesting pigments found in subsurface samples, as well as the more stable low-light (e.g., below MLD) and high-nutrient (all inorganic nutrients were more than double surface values) environment found under the ice and at the SCM (Table 2). Based on historical data, our results suggest that these properties are relatively consistent over the range of Arctic environments. It seems that the main difference between the environment sampled in ICESCAPE and that of past studies is the presence of thinner ice with more melt ponds than ever before. The increased light penetration through the sea ice created a near ideal environment for an under-ice phytoplankton bloom that set the pattern for the rest of the seasonal bloom cycle (Arrigo et al., in press).

The pattern of primary productivity in this region of the Arctic is one in which low light availability due to ice cover gradually gives way to nutrient-control of P-E parameters. Sea ice thinning has dramatically changed the underwater light field to allow for enhanced under-ice productivity, and importantly, has shifted the growing season to much earlier in the year. Furthermore, in this new paradigm, SCM-based production in the open water is a direct consequence of early season productivity under the ice, essentially meaning that the OW SCM is likely a remnant UI bloom (Arrigo et al., in press). As temperatures continue to warm and the ice continues to thin, the Pacific sector of the Arctic cannot solely be considered as a MIZ- and open-water–based productivity environment. New tools are needed to understand the significance and importance of under-ice and SCM-based primary production, as well as the consequences these shifting patterns of production have on the rest of the food web. Our data indicate that we may need to change our characterization of the seasonal Arctic bloom cycle, including placing more emphasis on under-ice productivity and modifying our understanding of SCM development. More research is needed to fully elucidate this process and the potential links between nutrients, light, and/or temperature in the under-ice environment.

Acknowledgments

We thank the officers and crew of the United States Coast Guard Cutter *Healy* for their assistance and support in the field; N. Bates for providing the dissolved inorganic carbon data; K. Frey for providing under ice light measurements; J. Swift and his team for providing nutrient data; A. C. Alderkamp for helpful comments during the writing of the manuscript; and the entire Impacts of Climate Change on the EcoSystems and Chemistry of the Arctic Pacific Environment (ICESCAPE) team, especially Z. W. Brown, A. Santiago, S. Martin, B. D. Schieber, and E. Weiss, for field and laboratory support. We also thank two anonymous reviewers for helpful comments in preparing the final manuscript.

This research is a contribution to the ICESCAPE project, which was sponsored by the Ocean Biology and Biogeochemistry and Cryospheric Sciences programs at National Aeronautics and Space Administration (NASA grant NNX10AF42G to K. R. Arrigo), and is also supported by NASA Earth and Space Science Fellowship grant NNX09AO48H to M. A. Palmer.

References

Arrigo, K. R., M. M. Mills, L. R. Kropuenske, G. L. van Dijken, A. C. Alderkamp, and D. H. Robinson. 2010. Photophysiology in two major Southern Ocean phytoplankton taxa: Productivity and growth of Phaeocystis antarctica and Fragilariopsis cylindrus under constant irradiance. Integr. Comp. Biol. **50:** 950–966, doi:10.1093/icb/icq021

———, and others. 2012. Massive phytoplankton blooms under Arctic sea ice. Science **336:** 1408, doi:10.1126/science.1215065

———, and ———. In press. Phytoplankton blooms beneath the sea ice in the Chukchi Sea. Deep-Sea Res. Part II (ICESCAPE Under Ice Bloom Special Issue).

———, and G. L. van Dijken. 2004. Annual cycles of sea ice and phytoplankton near Cape Bathurst, southeastern Beaufort Sea, Canadian Arctic. Geophys. Res. Lett. **31:** L08304, doi:10.1029/2003GL018978

———, and ———. 2011. Secular trends in Arctic Ocean net primary production. J. Geophys. Res. **116:** C09011, doi:10.1029/2011JC007151

———, ———, and S. Pabi. 2008. Impact of a shrinking Arctic ice cover on marine primary production. Geophys. Res. Lett. **35:** L19606, doi:10.1029/2008GL035063

Bates, N. R., M. H. P. Best, and D. A. Hansell. 2005. Spatiotemporal distribution of dissolved inorganic carbon and net community production in the Chukchi and Beaufort seas. Deep-Sea Res. Part II **52:** 3303–3323, doi:10.1016/j.dsr2.2005.10.005

Brugel, S. 2009. Étude des variations spatiales et temporelles du phytoplancton en mer de Beaufort : biomasse, production et structure de taille des communautés. Ph.D. thesis. Université du Québec à Rimouski. [Study on the spatial and temporal variability of phytoplankton in the Beaufort Sea: Biomass, production, and community structure.]

Carmack, E. C., D. G. Barber, J. Christensen, R. Macdonald, B. Rudels, and E. Sakshaug. 2006. Climate variability and physical forcing of the food webs and the carbon budget on Panarctic shelves. Prog. Oceanogr. **71:** 145–181, doi:10.1016/j.pocean.2006.10.005

———, R. W. Macdonald, and S. Jasper. 2004. Phytoplankton productivity on the Canadian Shelf of the Beaufort Sea. Mar. Ecol. Prog. Ser. **277:** 37–50, doi:10.3354/meps277037

Codispoti, L. A., C. N. Flagg, and J. H. Swift. 2009. Hydrographic conditions during the 2004 SBI process experiments. Deep-Sea Res. Part II **56:** 1144–1163, doi:10.1016/j.dsr2.2008.10.013

———, ———, V. Kelly, and J. H. Swift. 2005. Hydrographic conditions during the 2002 SBI process experiments. Deep-Sea Res. Part II **52:** 3199–3226, doi:10.1016/j.dsr2.2005.10.007

Comiso, J. C., C. L. Parkinson, R. Gersten, and L. Stock. 2008. Accelerated decline in the Arctic sea ice cover. Geophys. Res. Lett. **35:** L01703, doi:10.1029/2007GL031972

Cota, G. F. 1985. Photoadaptation of high Arctic ice algae. Nature **315:** 219–222, doi:10.1038/315219a0

———, L. R. Pomeroy, W. G. Harrison, E. P. Jones, F. Peters, W. M. Sheldon, Jr., and T. R. Weingartner. 1996. Nutrients, primary production and microbial heterotrophy in the southeastern Chukchi Sea: Arctic summer nutrient depletion and heterotrophy. Mar. Ecol. Prog. Ser. **135:** 247–258, doi:10.3354/meps135247

Falkowski, P. G. 1980. Light–shade adaptation in marine phytoplankton, p. 99–177. *In* P. G. Falkowski [ed.], Primary productivity in the sea. Plenum.

———. 1992. Molecular ecology of phytoplankton photosynthesis, p. 47–67. *In* P. G. Falkowski and A. Woodhead [eds.], Primary productivity and biogeochemical cycles in the sea. Plenum.

———, and J. LaRoche. 1991. Acclimation to spectral irradiance in algae. J. Phycol. **27:** 8–14, doi:10.1111/j.0022-3646.1991.00008.x

———, and T. G. Owens. 1980. Light–shade adaptation: two strategies in marine phytoplankton. Plant Physiol. **66:** 592–595, doi:10.1104/pp.66.4.592

———, and J. A. Raven. 2007. Aquatic photosynthesis, 2nd ed. Princeton Univ. Press.

Fortier, M., L. Fortier, C. Michel, and L. Legendre. 2002. Climatic and biological forcing of the vertical flux of biogenic particles under seasonal Arctic sea ice. Mar. Ecol. Prog. Ser. **225:** 1–16, doi:10.3354/meps225001

Frey, K. E., D. K. Perovich, and B. Light. 2011. The spatial distribution of solar radiation under a melting Arctic sea ice cover. Geophys. Res. Lett. **38:** L22501, doi:10.1029/2011GL049421

Grebmeier, J. M., L. W. Cooper, H. M. Feder, and B. I. Sirenko. 2006. Ecosystem dynamics of the Pacific-influenced Northern Bering and Chukchi seas in the Amerasian Arctic. Prog. Oceanogr. **71:** 331–361, doi:10.1016/j.pocean.2006.10.001

Hameedi, M. J. 1978. Aspects of water column primary productivity in the Chukchi Sea during summer. Mar. Biol. **48:** 37–48, doi:10.1007/BF00390529

Harrison, W. G., and G. F. Cota. 1991. Primary production in polar waters: relation to nutrient availability. Polar Res. **10:** 87–104, doi:10.1111/j.1751-8369.1991.tb00637.x

———, and T. Platt. 1986. Photosynthesis–irradiance relationships in polar and temperate phytoplankton populations. Polar Biol. **5:** 153–164, doi:10.1007/BF00441695

Hill, V., and G. Cota. 2005. Spatial patterns of primary production on the shelf, slope and basin of the Western Arctic in 2002. Deep-Sea Res. Part II **52:** 3344–3354, doi:10.1016/j.dsr2.2005.10.001

———, ———, and D. Stockwell. 2005. Spring and summer phytoplankton communities in the Chukchi and Eastern Beaufort seas. Deep-Sea Res. Part II **52:** 3369–3385, doi:10.1016/j.dsr2.2005.10.010

Kirk, J. T. O. 1994. Light and photosynthesis in aquatic ecosystems. Cambridge Univ. Press.

Kirst, G. O., and C. Wiencke. 1995. Ecophysiology of polar algae. J. Phycol. **31:** 181–199, doi:10.1111/j.0022-3646.1995.00181.x

Kropuenske, L. R., M. M. Mills, G. L. van Dijken, S. Bailey, D. H. Robinson, N. A. Welschmeyer, and K. R. Arrigo. 2009. Photophysiology in two major Southern Ocean phytoplankton taxa: Photoprotection in *Phaeocystis antarctica* and *Fragilariopsis cylindrus*. Limnol. Oceanogr. **54:** 1176–1196, doi:10.4319/lo.2009.54.4.1176

Lee, S. H., D. Stockwell, and T. E. Whitledge. 2010. Uptake rates of dissolved inorganic carbon and nitrogen by under-ice phytoplankton in the Canada Basin in summer 2005. Polar Biol. **33:** 1027–1036, doi:10.1007/s00300-010-0781-4

Legendre, L., R. G. Ingram, and M. Poulin. 1981. Physical control of phytoplankton production under sea ice (Manitounuk Sound, Hudson Bay). Can. J. Fish. Aquat. Sci. **38:** 1385–1392, doi:10.1139/f81-185

Lewis, M. R., and J. C. Smith. 1983. A small volume, short-incubation-time method for measurement of photosynthesis as a function of incident irradiance. Mar. Ecol. Prog. Ser. **13:** 99–102, doi:10.3354/meps013099

Li, W. K. W., F. A. McLaughlin, C. Lovejoy, and E. C. Carmack. 2009. Smallest algae thrive as the Arctic Ocean freshens. Science **326:** 539, doi:10.1126/science.1179798

———, J. C. Smith, and T. Platt. 1984. Temperature response of photosynthetic capacity and carboxylase activity in Arctic marine phytoplankton. Mar. Ecol. Prog. Ser. **17:** 237–243, doi:10.3354/meps017237

Lindsay, R. W., and J. Zhang. 2005. The thinning of Arctic sea ice, 1988–2003: Have we passed a tipping point? J. Climate **18:** 4879–4894, doi:10.1175/JCLI3587.1

Loeng, H., and others. 2005. Marine systems, p. 453–538. *In* C. Symon, L. Arris, and B. Heal [eds.], Arctic climate impact assessment. Cambridge Univ. Press.

MacIntyre, H. L., T. M. Kana, T. Anning, and R. J. Geider. 2002. Photoacclimation of photosynthesis irradiance response curves and photosynthetic pigments in microalgae and cyanobacteria. J. Phycol. **38:** 17–38, doi:10.1046/j.1529-8817.2002.00094.x

Maslanik, J., J. Stroeve, C. Fowler, and W. Emery. 2011. Distribution and trends in Arctic sea ice age through spring 2011. Geophys. Res. Lett. **38:** L13502, doi:10.1029/2011GL047735

Martin, J. J.-È., and others. 2010. Prevalence, structure and properties of subsurface chlorophyll maxima in Canadian Arctic waters. Mar. Ecol. Prog. Ser. **412:** 69–84, doi:10.3354/meps08666

Mitchell, B. G., M. Kahru, J. Wieland, and M. Stramska. 2002. Determination of spectral absorption coefficients of particles, dissolved material and phytoplankton for discrete water samples, p. 39–64. *In* J. L. Mueller, G. S. Fargion, and C. R. McClain [eds.], Ocean optics protocols for satellite ocean color sensor validation, Rev. 4, Vol. IV, NASA Tech. Memo. NASA/TM-2003-211621/Rev4-Vol.IV.

Morel, A., and A. Bricaud. 1981. Theoretical results concerning light absorption in a discrete medium, and application to specific absorption of phytoplankton. Deep-Sea Res **28:** 1375–1393, doi:10.1016/0198-0149(81)90039-X

Morgan-Kiss, R. M., J. C. Priscu, T. Pocock, L. Gudynaite-Savitch, and N. P. A. Hunter. 2006. Adaptation and acclimation of photosynthetic microorganisms to permanently cold environments. Microbiol. Mol. Biol. Rev. **70:** 222–252, doi:10.1128/MMBR.70.1.222-252.2006

Mundy, C. J., and others. 2009. Contribution of under-ice primary production to an ice-edge upwelling phytoplankton bloom in the Canadian Beaufort Sea. Geophys. Res. Lett. **36:** L17601, doi:10.1029/2009GL038837

Nghiem, S. V., I. G. Rigor, D. K. Perovich, P. Clemente-Colon, J. W. Weatherly, and G. Neumann. 2007. Rapid reduction of Arctic perennial sea ice. Geophys. Res. Lett. **34:** L19504, doi:10.1029/2007GL031138

Pabi, S., G. L. van Dijken, and K. R. Arrigo. 2008. Primary production in the Arctic Ocean, 1998–2006. J. Geophys. Res. **113:** C08005, doi:10.1029/2007JC004578

Palmer, M. A., and others. 2011. Spatial and temporal variation of photosynthetic parameters in natural phytoplankton assemblages in the Beaufort Sea, Canadian Arctic. Polar Biol. **34:** 1915–1928, doi:10.1007/s00300-011-1050-x

Perovich, D. K. 1998. Physics of ice covered seas, v. 1. Univ. of Helsinki Press.

———, and C. Polashenski. 2012. Albedo evolution of seasonal Arctic sea ice. Geophys. Res. Lett. **39:** L08501, doi:10.1029/2012GL051432

Perrette, M., A. Yool, G. D. Quartly, and E. E. Popova. 2011. Near-ubiquity of ice-edge blooms in the Arctic. Biogeosciences **8:** 515–524, doi:10.5194/bg-8-515-2011

Pickart, R. S. 2004. Shelf break circulation in the Alaskan Beaufort Sea: Mean structure and variability. J. Geophys. Res. **109:** C04024, doi:10.1029/2003JC001912

Platt, T., C. L. Gallegos, and W. G. Harrison. 1980. Photoinhibition of photosynthesis in natural assemblages of marine phytoplankton. J. Mar. Res. **38:** 687–701.

———, W. G. Harrison, B. Irwin, E. P. Horne, and C. L. Gallegos. 1982. Photosynthesis and photoadaptation of marine phytoplankton in the Arctic. Deep-Sea Res. **29:** 1159–1170, doi:10.1016/0198-0149(82)90087-5

Rothrock, D. A., Y. Yu, and G. A. Maykut. 1999. Thinning of Arctic sea-ice cover. Geophys. Res. Lett. **26:** 3469–3472.

Sakshaug, E. 2004. Primary and secondary production in Arctic seas, p. 57–81. *In* R. Stein and R. W. Macdonald [eds.], The organic carbon cycle in the Arctic Ocean. Springer-Verlag.

Shirasawa, K., H. Eicken, K. Tateyama, T. Takatsuka, and T. Kawamura. 2009. Sea ice thickness variability in the Chukchi Sea, spring and summer 2002–2004. Deep-Sea Res. Part II **56:** 1182–1200, doi:10.1016/j.dsr2.2008.10.015

SooHoo, J. B., A. C. Palmisano, S. T. Kottmeier, M. P. Lizotte, S. L. SooHoo, and C. W. Sullivan. 1987. Spectral light absorption and quantum yield of photosynthesis in sea ice microalgae and a bloom of *Phaeocystis pouchetii* from McMurdo Sound, Antarctica. Mar. Ecol. Prog. Ser. **39:** 175–89, doi:10.3354/meps039175

Stirling, I. 1997. The importance of polynyas, ice edges, and leads to marine mammals and birds. J. Mar. Sys. **10:** 9–21, doi:10.1016/S0924-7963(96)00054-1

Stroeve, J. S., M. C. Sereeze, F. Fetterer, T. Arbetter, W. Meier, J. Maslanik, and K. Knowles. 2005. Tracking the Arctic's shrinking ice cover: Another extreme September minimum in 2004. Geophys. Res. Lett. **32:** L04501.1–L04501.4, doi:10.1029/2004GL021810

Subba Rao, D. V., and T. Platt. 1984. Primary production of Arctic waters. Polar Biol. **3:** 191–201, doi:10.1007/BF00292623

Sukenik, A., J. Bennett, and P. G. Falkowski. 1987. Light-saturated photosynthesis—limitation by electron transport or carbon fixation. Biochim. Biophys. Acta **891:** 205–215, doi:10.1016/0005-2728(87)90216-7

Tremblay, J.-É., C. Michel, K. A. Hobson, M. Gosselin, and N. M. Price. 2006. Bloom dynamics in early opening waters of the Arctic Ocean. Limnol. Oceanogr. **51:** 900–012, doi:10.4319/lo.2006.51.2.0900

———, K. Simpson, J. Martin, L. A. Miller, Y. Gratton, D. G. Barber, and N. M. Price. 2008. Vertical stability and the annual dynamics of nutrients and chlorophyll fluorescence in the coastal, southeast Beaufort Sea. J. Geophys. Res. **113:** C07S90, doi:10.1029/2007JC004547

Wang, J., G. F. Cota, and J. Comiso. 2005. Phytoplankton in the Beaufort and Chukchi seas: Distribution, dynamics, and environmental forcing. Deep-Sea Res. Part II **52:** 3355–3368, doi:10.1016/j.dsr2.2005.10.014

Wassmann, P. 2006. Structure and function of contemporary food webs on Arctic shelves: An introduction. Prog. Oceanogr. **71:** 123–128, doi:10.1016/j.pocean.2006.09.008

Zhang, J., Y. H. Spitz, M. Steele, C. Ashjian, R. Campbell, L. Berline, and M. Matrai. 2010. Modeling the impact of declining sea ice on the Arctic marine planktonic ecosystem. J. Geophys. Res. **115:** C10015, doi:10.1029/2009JC005387

Associate editor: Robert R. Bidigare

Received: 28 February 2013
Accepted: 30 July 2013
Amended: 20 August 2013